Thermo-viscous damping of acoustic waves in narrow channels: A comparison of effects in air and water

Philip A. Cotterill, David Nigro, I. David Abrahams, Erik Garcia-Neefjes, and William J. Parnell

Citation: The Journal of the Acoustical Society of America **144**, 3421 (2018); doi: 10.1121/1.5078528
View online: https://doi.org/10.1121/1.5078528
View Table of Contents: https://asa.scitation.org/toc/jas/144/6
Published by the Acoustical Society of America

Thermo-viscous damping of acoustic waves in narrow channels: A comparison of effects in air and water

Philip A. Cotterill,[1] David Nigro,[2] I. David Abrahams,[3] Erik Garcia-Neefjes,[1] and William J. Parnell[1,a)]

[1]*School of Mathematics, University of Manchester, Oxford Road, Manchester, M13 9PL, United Kingdom*
[2]*Thales United Kingdom, 350 Longwater Avenue Green Park, Reading, RG2 6GF, United Kingdom*
[3]*Isaac Newton Institute, University of Cambridge, Clarkson Road, Cambridge, CB3 0EH, United Kingdom*

(Received 8 March 2018; revised 16 October 2018; accepted 21 October 2018; published online 21 December 2018)

Recent work in the acoustic metamaterial literature has focused on the design of metasurfaces that are capable of absorbing sound almost perfectly in narrow frequency ranges by coupling resonant effects to visco-thermal damping within their microstructure. Understanding acoustic attenuation mechanisms in narrow, viscous-fluid-filled channels is of fundamental importance in such applications. Motivated by recent work on acoustic propagation in narrow, air-filled channels, a theoretical framework is presented that demonstrates the controlling mechanisms of acoustic propagation in arbitrary Newtonian fluids, focusing on attenuation in air and water. For rigid-walled channels, whose widths are on the order of Stokes's boundary layer thickness, attenuation in air at 10 kHz can be over 200 dB m^{-1}; in water it is less than 37 dB m^{-1}. However, in water, fluid-structure-interaction effects can increase attenuation dramatically to over 77 dB m^{-1} for a steel-walled channel, with a reduction in phase-speed approaching 70%. For rigid-walled channels, approximate analytical expressions for dispersion relations are presented that are in close agreement with exact solutions over a broad range of frequencies, revealing explicitly the relationship between complex phase-speed, frequency and channel width.

https://doi.org/10.1121/1.5078528

[BA] Pages: 3421–3436

I. INTRODUCTION

Perforations in plates and structures have traditionally been used as a sound manipulation tool (Estrada *et al.*, 2008; Leppington and Levine, 1973; Putra and Thompson, 2010) with a significant breadth of work having been carried out over the years, involving analytical, computational, and experimental approaches. This research has been performed mainly in order to study the influence of microstructure on transmission and reflection of incident acoustic energy. In recent years the term *metasurface* has been coined by the metamaterials community, as a microstructured surface that is capable of almost complete absorption of sound, usually in a very narrowband manner with some of the microstructure proposed being quite *exotic* (Jiménez *et al.*, 2017; Jiménez *et al.*, 2016). A classical related problem, still of great importance and studied with significant interest, is the problem of acoustic propagation through a screen with periodic slits or channels (Christensen *et al.*, 2008). The canonical problem of transmission through a single channel, slit, or duct with rigid walls has been studied widely over the years (Allard and Atalla, 2009; Gomperts and Kihlman, 1967; Gompeters, 1964; Oldham and Zhao, 1993; Stinson and Champoux, 1992; Wilson and Soroka, 1965). It is well-known that resonances are set up within the channel, associated with relations between the wavelength and the length of the slit, save for what are known as *end-corrections*. Although the term has not classically been employed, more recently these resonances have been termed the *Fabry-Perot* resonances, terminology that appears to have crossed over from the electromagnetics community. Christensen *et al.* (2008) provided a model for the emergence of such resonances associated with an inviscid fluid. As pointed out by Ward *et al.* (2015), however, neglecting thermo-viscous effects is a significant assumption, particularly at small lengthscales and the latter authors showed that including attenuation *in-air* results in the phase speed along a narrow duct or channel being substantially reduced, even when the channel width is an order of magnitude greater than the boundary layer parameter $\bar{\delta}_\nu = \sqrt{\bar{\nu}/\bar{\omega}}$. Here $\bar{\nu}$ denotes kinematic viscosity and $\bar{\omega}$ is the radian frequency. In the present analysis, we show that Stokes's boundary layer thickness $\bar{\delta}_s = 2\pi\sqrt{2\bar{\nu}/\bar{\omega}} \approx 9\bar{\delta}_\nu$ is a better indicator than $\bar{\delta}_\nu$ of the extent to which the channel-wall boundary layers disturb the motion of the fluid; $\bar{\delta}_\nu$ underestimates, somewhat, the true extent of the boundary layer.

More generally then, over the years it has been observed that thermo-viscous boundary layer effects can have a significant impact upon the propagation of sound along narrow, rigid-walled channels giving substantial acoustic absorption within the audio frequency range in air. This phenomenon is used routinely in the acoustics industry as a means to *soften*

a)Electronic mail: william.parnell@manchester.ac.uk

boundaries and attenuate unwanted sound. Indeed, the propagation of acoustic waves along channels, ducts, tubes, or slits has been studied extensively over the years, with work dating back to the late nineteenth century. Helmholtz (1863) studied the impact of viscosity and estimated the absorption due to viscous effects. Kundt (1868) tested the theory experimentally and noticed that absorption was higher than expected, presumably due to thermal effects. Kirchhoff (1868) introduced the general theory of thermo-visco acoustics based on the Navier-Stokes equations and the Fourier-law of heat conduction for a perfect gas in a circular tube. He also gave approximate expressions in the case of a *wide* tube, i.e., when the radius is much larger than the viscous/thermal boundary layer thickness. Rayleigh (1896) gave approximate solutions for the *narrow* tube limit, i.e., when the radius is much smaller than the viscous/thermal boundary layer thickness and for the two-dimensional narrow channel case. Zwikker and Kosten (1949) introduced an approximate model for *wide* tubes that allowed for the derivation of a simpler solution in which viscous and thermal effects decoupled. Weston (1953), based on Kirchhoff's model, developed approximations for tubes of various diameters (*narrow*, *wide*, and *very wide*). Tijdeman (1975) rewrote Kirchhoff's model in terms of non-dimensionalized parameters, which allowed him to estimate the relative importance of each term and to show that the two main factors involved are the reduced viscous wavenumber and the reduced acoustic wavenumber. Bruneau *et al.* (1989) presented a general framework for a perfect gas in a bounded domain; a general formula for the dispersion relation with a no-slip boundary condition for the velocity and an isothermal boundary condition for the temperature is obtained and applied to simple geometries. Stinson (1991) analyzed Kirchhoff's original model and showed that Zwikker and Kosten's solution is recovered in the appropriate limit. He also extended Kirchhoff's theory to tubes of arbitrary cross-section. Beltman (1999a) provided an extensive literature review on the various models and approximations developed in thermo-viscous acoustics for a perfect gas. All those models were compared and their domain of validity was assessed. Solutions for canonical problems for each approximate/exact model were also provided. In subsequent work, this theory was then applied to a variety of engineering problems, such as the spherical resonator, the classic circular tube, and a miniaturized acoustic transducer (Beltman, 1999b). The last model is of particular interest as it involved a fluid-structure interaction problem.

It is clear that most, if not all, the literature above is focused on a perfect gas. The study of thermo-viscous acoustic propagation in *narrow water filled channels* or *slits* appears to be lacking although work has been done on the viscous liquid-filled elastic tube, usually having relatively thin walls. This area of research was initiated by Del Grosso (1971) who considered multimode propagation in an inviscid fluid-filled elastic tube. It has been followed up recently with work that includes viscous effects, carried out in a number of papers (Baik *et al.*, 2010; Dokumaci, 2014; Elvira-Segura, 2000; Liangh and Scarton, 2002). We note, however, that the frequency range considered in these works is generally high since the studies are mainly associated with non-destructive evaluation. The low frequency regime appears to be unexplored territory.

The purpose of the analysis presented in this paper is therefore two-fold, first to provide a general framework with which to study thermo-viscous acoustic attenuation in narrow channels that is applicable to an arbitrary Newtonian fluid. In particular, we wish to study the impact of thermo-viscous effects upon dense fluids of low compressibility, for which the *perfect gas* assumption is clearly inappropriate, and to determine the extent to which boundary layer influences are felt throughout the channel both in air and in water. Second, we wish to determine the conditions under which viscous and thermal boundary effects may influence acoustic propagation in water, when account is taken of the coupling between water and a real (elastic) channel wall material. (A pre-requisite to this study is the development of a theoretical framework for a general Newtonian fluid.) In the present study, we restrict our attention to the influence of thermo-viscous effects upon the lowest order symmetric duct mode, as only this mode would propagate along a narrow, rigid-walled tube filled with an inviscid fluid; future studies will consider higher-order modes.

In Sec. II we summarize the equations that arise when Beltman's analysis is extended to an arbitrary Newtonian fluid by using the linearized, quasi-equilibrium equations of state for a viscous fluid presented in Chapter 3 of Dunn *et al.* (2015), thereby enabling the study of the impact of thermo-viscous effects upon sound propagation in water. These equations are then applied to study the propagation of sound in narrow rigid-walled two-dimensional channels in Sec. III, where analytic expressions are derived for the dispersion equations of natural modes incorporating thermo-viscous effects. From this analysis, we are able to determine the conditions under which thermo-viscosity has a significant impact upon the propagation of guided acoustic waves by examining the phase-speed and attenuation of such waves along the channel for two different thermal boundary conditions: insulating and conducting. In particular, we show that the thermal expansion coefficient of the fluid has a significant impact upon the relative influence of viscous and thermal effects.

In Sec. IV we present results associated with propagation in air and in water along rigid-walled channels, and consider the different behavior of these two fluids. We show that their behaviors are captured by simple approximate analytic expressions for the complex phase-speed that are valid up to the MHz frequency range. We also compare our theoretical predictions to the in-air measurements of Ward *et al.* (2015) and find that our results are broadly consistent with their data, thereby confirming our analysis, which should be valid for any simple (Newtonian) fluid. Finally, in Sec. V, we consider acoustic coupling with compliant boundaries. As is known this is particularly important in the water-filled channel, unlike the air-filled case where all boundaries can, in general, be considered rigid. In particular, we show that for narrow, water-filled channels that have widths of the same order of magnitude as Stokes's boundary layer thickness, fluid-structure interaction has a dramatic impact upon the characteristics of the fundamental acoustic mode of propagation. Attenuation is increased by about 40 dB m^{-1} compared to the

rigid-walled assumption and the phase speed is slowed by almost 70%. We offer conclusions in Sec. VI.

Whilst variables and parameters employed herein are defined in the text, where they are first encountered, a notation summary is provided in the Appendix for the convenience of the reader.

II. GOVERNING EQUATIONS FOR THERMO-VISCOUS ACOUSTICS

In this section, the equations governing linear thermo-viscous acoustics are presented in non-dimensional form. By combining these equations in the manner described by Beltman (1999a), for time-harmonic propagation, the vorticity field is shown to satisfy the Helmholtz equation and fractional temperature fluctuations of the fluid can be described by a pair of Helmholtz equations. From these solutions the velocity and pressure fields can be constructed. The study is restricted to two dimensions, which is appropriate for the models of interest.

A. Thermo-viscous fluids

Below we state the linearized governing equations for thermo-viscous fluids with dimensional variables and parameters having an over-bar and their non-dimensional counterparts being free of bars. In non-dimensional form then, these equations are (see, e.g., Chapter 3 of Dunn *et al.*, 2015)

$$\frac{\partial s}{\partial t} + \nabla \cdot \boldsymbol{u} = 0, \tag{1}$$

$$\frac{\partial \boldsymbol{u}}{\partial t} = -\nabla p + \eta \nabla^2 \boldsymbol{u} + (\eta + \eta')\nabla(\nabla \cdot \boldsymbol{u}), \tag{2}$$

$$\frac{\partial \theta}{\partial t} - \frac{\mathcal{K}}{c_p}\nabla^2\theta - \frac{\beta}{c_p}\frac{\partial p}{\partial t} = 0, \tag{3}$$

$$s = p - \frac{\beta}{c_p}h, \quad \theta = \frac{1}{c_p}(\beta p + h), \tag{4}$$

where boldface symbols are used to denote vector quantities. h denotes non-dimensionalized fluctuations of entropy per unit mass, whilst p is the non-dimensional acoustic pressure. They are defined by

$$p = \frac{\bar{p} - \bar{p}_0}{\bar{\rho}_0 \bar{c}_0^2}, \quad h = \frac{\bar{T}_0}{\bar{c}_0^2}(\bar{h} - \bar{h}_0). \tag{5}$$

s and θ are, respectively, the fractional fluctuations of density and temperature, i.e.,

$$s = \frac{\bar{\rho} - \bar{\rho}_0}{\bar{\rho}_0}, \quad \theta = (\bar{T} - \bar{T}_0)/\bar{T}_0. \tag{6}$$

In the above, $\bar{p}$, $\bar{\rho}$, $\bar{h}$, and $\bar{T}$ denote, respectively, the fluctuating (dimensional) pressure, density, entropy, and absolute temperature of the fluid, with $\bar{p}_0$, $\bar{\rho}_0$, $\bar{h}_0$, and $\bar{T}_0$ being their equilibrium values (taken to be spatially invariant); $\bar{c}_0$ is the barotropic sound speed of the fluid. Other relations between dimensional and non-dimensional variables are those for the fluid particle velocity $\bar{\boldsymbol{u}} = \bar{c}_0 \boldsymbol{u} = \bar{c}_0 (u_x, u_y, 0)$, Cartesian variables $(\bar{x}, \bar{y}) = \bar{\mathcal{L}}(x, y)$ where $\bar{\mathcal{L}}$ is a problem specific length scale and time $\bar{t} = (\bar{\mathcal{L}}/\bar{c}_0)\, t$. Non-dimensional parameters are also introduced for convenience, in particular the first, or shear, coefficient of viscosity: $\bar{\eta} = \bar{\rho}_0 \bar{c}_0 \bar{\mathcal{L}}\, \eta$ and second coefficient of viscosity: $\bar{\eta}' = \bar{\rho}_0 \bar{c}_0 \bar{\mathcal{L}}\, \eta'$, noting that $\bar{\eta}$ and $\bar{\eta}'$ are related to the commonly used bulk viscosity, $\bar{\eta}_B$, through $\bar{\eta}_B = \bar{\eta}' + (2/3)\bar{\eta}$. Furthermore, the thermodynamic coefficients of conductivity $\bar{\mathcal{K}}$, specific heat at constant pressure $\bar{c}_p$, and thermal expansion at constant pressure $\bar{\beta}$ are non-dimensionalized as follows:

$$\mathcal{K} = \frac{\bar{T}_0 \bar{\mathcal{K}}}{\bar{\rho}_0 \bar{c}_0^3 \bar{\mathcal{L}}}, \quad c_p = \frac{\bar{T}_0}{\bar{c}_0^2}\bar{c}_p, \quad \beta = \bar{\beta}\bar{T}_0. \tag{7}$$

Equation (2) is associated with a non-dimensional viscous stress tensor, which, in index form, has an ijth component (see, e.g., Chapter 41 of Feynman *et al.*, 1965)

$$\sigma_{ij} = \eta\left(\frac{\partial u_i}{\partial x_j} + \frac{\partial u_j}{\partial x_i}\right) + \eta' \delta_{ij}\frac{\partial u_k}{\partial x_k}, \tag{8}$$

where $u_1 \equiv u_x$, $u_2 \equiv u_y$, $x_1 \equiv x$, $x_2 \equiv y$, δ_{ij} is the ijth component of the Kronecker-delta tensor and we employ the convention that repeated indices are summed over. The dimensional stress is $\bar{\sigma}_{ij} = \bar{\rho}_0 \bar{c}_0^2 \sigma_{ij}$.

B. Decomposition into vortex and thermo-compression fields

Beltman (1999a) shows that the governing equations for an ideal gas decouple into a vortex field, $\boldsymbol{\Omega}$, and two thermo-compression fields, Θ_1 and Θ_2. We find this field description to be valid in the more general case of an arbitrary Newtonian fluid whose governing equations were described in the previous section. The decomposition applied to an arbitrary Newtonian fluid within the frequency domain is given next as well as the relationships between $\boldsymbol{\Omega}$, Θ_1, Θ_2, and other variables.

Since the problem here is considered two-dimensional, the vortex field can be written as $\boldsymbol{\Omega} = \nabla \times \boldsymbol{u} = \hat{\boldsymbol{k}}\Omega$, where $\hat{\boldsymbol{k}}$ indicates a unit vector pointing in the z-direction, and Ω is a scalar function. Ω satisfies the diffusion equation

$$\frac{\partial \Omega}{\partial t} = \eta \nabla^2 \Omega, \tag{9}$$

and is decoupled from the thermal and compression field-variables. For harmonic excitation, $\Omega(x,y,t) = \tilde{\Omega}(x,y,\omega)e^{-i\omega t}$, where $\omega = \bar{\omega}\bar{\mathcal{L}}/\bar{c}_0$ is the non-dimensionalized frequency (or equivalently non-dimensionalized acoustic wavenumber), and Eq. (9) becomes the complex Helmholtz equation for $\tilde{\Omega}$, i.e.,

$$\left(\nabla^2 + \frac{i\omega}{\eta}\right)\tilde{\Omega} = 0. \tag{10}$$

In terms of dimensional parameters,

$$\frac{\omega}{\eta} = \left(\frac{\bar{\mathcal{L}}}{\bar{\delta}_\nu}\right)^2, \tag{11}$$

where $\bar{\delta}_\nu$ is the boundary layer parameter of Ward *et al.* (2015) that was referred to in the Introduction.

Similarly, harmonic temperature fluctuations are written as $\theta(x,y,t) = \tilde{\theta}(x,y,\omega)e^{-i\omega t}$, where the following decomposition is used for $\tilde{\theta}$:

$$\tilde{\theta}(x,y,\omega) = \tilde{\Theta}_1(x,y,\omega) + \tilde{\Theta}_2(x,y,\omega). \tag{12}$$

$\tilde{\Theta}_1(x,y,\omega)$ and $\tilde{\Theta}_2(x,y,\omega)$ each satisfy a Helmholtz equation, viz.,

$$(\nabla^2 + \kappa_1^2)\tilde{\Theta}_1 = 0, \quad (\nabla^2 + \kappa_2^2)\tilde{\Theta}_2 = 0, \tag{13}$$

where

$$\kappa_1^2 = i\omega\,\frac{[1 - i\omega(\zeta + \mathcal{AC})] + \mathcal{S}}{2(1 - i\omega\zeta\mathcal{A})\mathcal{C}},$$
$$\kappa_2^2 = i\omega\,\frac{[1 - i\omega(\zeta + \mathcal{AC})] - \mathcal{S}}{2(1 - i\omega\zeta\mathcal{A})\mathcal{C}}, \tag{14}$$

with

$$\mathcal{S} = \sqrt{[1 - i\omega(\zeta - \mathcal{AC})]^2 - 4i\omega\,\mathcal{C}(\mathcal{A} - 1)},$$
$$\mathcal{A} = 1 + \frac{\beta^2}{c_p}, \quad \mathcal{C} = \frac{\mathcal{K}}{c_p}, \tag{15}$$

and $\zeta = 2\eta + \eta' = \eta_B + (4/3)\eta$. $\mathcal{C}$ represents the non-dimensionalized thermal diffusion coefficient. If in Eq. (14) and the first of Eq. (15), $\mathcal{A}$ is replaced by the ratio of specific heats at constant pressure and volume, the solution for an ideal gas is recovered; see, for example, Stinson (1991) and Beltman (1999a).

It is readily shown for harmonic excitation, defining the velocity $\boldsymbol{u}(x,y,t) = \tilde{\boldsymbol{u}}(x,y,\omega)e^{-i\omega t}$, condensation $s(x,y,t) = \tilde{s}(x,y,\omega)e^{-i\omega t}$ and pressure $p(x,y,t) = \tilde{p}(x,y,\omega)e^{-i\omega t}$, that these harmonic variables can be defined in terms of $\tilde{\Omega}, \tilde{\Theta}_1$ and $\tilde{\Theta}_2$ in the forms

$$i\omega\tilde{\boldsymbol{u}} = \frac{c_p}{2\beta}\{[1 - i\omega(\zeta - \mathcal{AC}) - \mathcal{S}]\nabla\tilde{\Theta}_1 + [1 - i\omega(\zeta - \mathcal{AC}) + \mathcal{S}]\nabla\tilde{\Theta}_2\} + \eta\nabla\times\hat{\boldsymbol{k}}\tilde{\Omega}, \tag{16}$$

$$\tilde{s} = \frac{c_p}{\beta}\left[\left(1 + i\frac{\mathcal{AC}\kappa_1^2}{\omega}\right)\tilde{\Theta}_1 + \left(1 + i\frac{\mathcal{AC}\kappa_2^2}{\omega}\right)\tilde{\Theta}_2\right], \tag{17}$$

$$\tilde{p} = \frac{c_p}{\beta}\left[\left(1 + i\frac{\mathcal{C}\kappa_1^2}{\omega}\right)\tilde{\Theta}_1 + \left(1 + i\frac{\mathcal{C}\kappa_2^2}{\omega}\right)\tilde{\Theta}_2\right]. \tag{18}$$

Having summarized the governing equations and relations between dependent field variables, we now move on to defining the problem of interest.

III. THERMO-VISCOUS ACOUSTIC PROPAGATION IN NARROW CHANNELS WITH RIGID WALLS

In this section and with reference to Fig. 1, we examine the behavior of the natural modes of propagation along an infinitely-long parallel-sided channel, considering the impact of frequency, and channel width in particular, upon phase-speed and attenuation. The channel is aligned with the x-direction and lies in $|\bar{y}| \le \bar{L}$. Its width in the z-direction is considered to be of infinite extent, and the motion of the fluid is considered to be independent of $\bar{z}$. Hence, the problem is two dimensional, governed by the equations summarized in Sec. II.

We start by setting the characteristic length scale, $\bar{\mathcal{L}} = \bar{L}$, i.e., equal to the half-width of the channel. Thus, in non-dimensional coordinates, the channel lies in $|y| \le 1$ and is aligned along the x direction. Its walls are considered rigid so that

$$\tilde{\boldsymbol{u}}(x, y = \pm 1, \omega) = 0. \tag{19}$$

Solutions are sought with the dependence e^{ikx}, where k may be complex [with $\Im(k) \ge 0$] and its permissible values are determined by the boundary conditions on the channel wall. Here we concentrate upon natural modes possessing a symmetric pressure distribution about the centre-line of the channel. This case is of particular interest because, for an inviscid fluid, only the lowest order *symmetric* mode is cut on at channel widths and frequencies of interest; all other modes are evanescent. For symmetric modes, we require $\tilde{p}(x,y,\omega)$ to be an even function of y. This requires $\tilde{s}$, $\tilde{\theta}$, and $\tilde{u}_x$ to be even functions of y, whilst $\tilde{\Omega}$ and $\tilde{u}_y$ are odd. Hence our basic k-space solutions for temperature and vorticity, which we denote by $\hat{\theta}(k,y,\omega) = \hat{\Theta}_1(k,y,\omega) + \hat{\Theta}_2(k,y,\omega)$, and $\hat{\Omega}(k,y,\omega)$, respectively, using the hat symbol to denote a k-space function, take the forms

$$\hat{\theta}(k,y,\omega) = B(k,\omega)\cosh(\gamma_1 y) + D(k,\omega)\cosh(\gamma_2 y), \tag{20}$$

$$\hat{\Omega}(k,y,\omega) = E(k,\omega)\sinh(\alpha y), \tag{21}$$

where $\gamma_1 = (k^2 - \kappa_1^2)^{1/2}, \gamma_2 = (k^2 - \kappa_2^2)^{1/2}, \alpha = (k^2 - i\omega/\eta)^{1/2}$. The functional forms of B, D, and E will clearly depend upon the thermal properties of the channel walls. We now consider two cases: thermally insulating walls and isothermal (perfectly conducting) walls.

In addition to Eq. (19), a *thermally insulating channel wall* must also satisfy

$$\frac{\partial\tilde{\theta}}{\partial y}(x, y = \pm 1, \omega) = 0, \tag{22}$$

or its equivalent form in k-space. Imposing the boundary conditions in Eqs. (19) and (22) upon the basic solutions

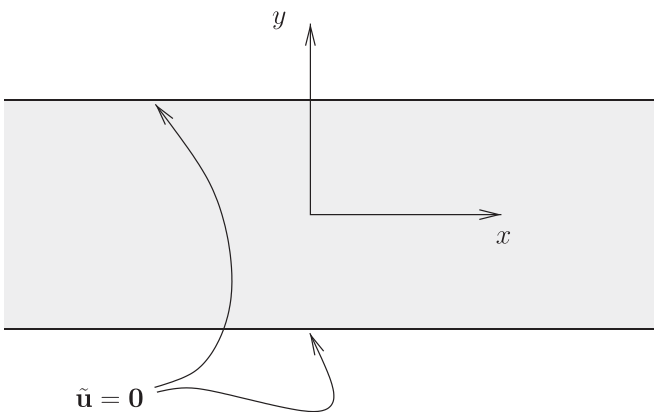

FIG. 1. Thermo-viscous acoustic propagation in a channel, running parallel to the x axis and having rigid walls at $y = \pm 1$.

from Eqs. (20) and (21), noting Eq. (16), requires that for natural modes of propagation along the channel, k must satisfy the following dispersion equation:

$$k^2\tanh(\alpha)\{\,[1-i\omega(\zeta-\mathcal{AC})-\mathcal{S}]\gamma_2\tanh(\gamma_2) -[1-i\omega(\zeta-\mathcal{AC})+\mathcal{S}]\gamma_1\tanh(\gamma_1)\,\} + 2\alpha\gamma_1\gamma_2\mathcal{S}\tanh(\gamma_1)\tanh(\gamma_2)=0. \tag{23}$$

Temperature fluctuations vanish on a *perfectly conducting channel wall* whose temperature is maintained at the equilibrium temperature of the fluid. Thus, the thermal boundary condition for this case is

$$\tilde{\theta}(x,y=\pm1,\omega)=0, \tag{24}$$

with the corresponding dispersion equation for *symmetric* modes being

$$\alpha\{\,[1-i\omega(\zeta-\mathcal{AC})-\mathcal{S}]\gamma_1\tanh(\gamma_1) -[1-i\omega(\zeta-\mathcal{AC})+\mathcal{S}]\gamma_2\tanh(\gamma_2)\} + 2k^2\mathcal{S}\tanh(\alpha)=0. \tag{25}$$

A. The limit of zero thermal expansion

In Sec. IV below, we examine the numerical behavior of the dispersion equation for typical values of the thermo-viscous coefficients applicable to air and water. First, however, it is instructive to consider the limit of vanishingly small thermal expansion, which is of particular relevance to water.

It is clear from Eq. (4) that for a vanishingly small thermal expansion coefficient, pressure and density variations are decoupled from temperature fluctuations. That is as $\beta\to0$,

$$s\to p,\quad \theta\to\frac{h}{c_p}, \tag{26}$$

and the acoustic (compressional) channel modes become independent of thermal effects but may still be influenced by the viscous boundary layer. In this limit, we see from Eq. (15) that clearly $\mathcal{A}=1+O(\beta^2)$, and $\mathcal{S}\to1-i\omega(\zeta-\mathcal{C})+O(\beta^2)$, whence Eqs. (23) and (25) acquire the following common form:

$$\mathcal{D}_{vr}=k^2\tanh(\alpha)-\alpha\gamma_2\tanh(\gamma_2)=0. \tag{27}$$

Equation (27) is independent of γ_1 and hence κ_1, where in the limit $\beta\to0$, κ_1 depends only upon thermal parameters (and fluid density), indeed

$$\kappa_1\to\sqrt{\frac{i\omega}{\mathcal{C}}}\left[1+O\left(\beta^2\right)\right]\quad\text{as }\beta\to0, \tag{28}$$

whilst

$$\kappa_2\to\frac{\omega}{\sqrt{1-i\omega\zeta}}\left[1+O\left(\beta^2\right)\right]\quad\text{as }\beta\to0, \tag{29}$$

which depends only upon viscous and acoustic parameters. Furthermore, as $\beta\to0$, Eqs. (16) to (18) acquire the following forms:

$$i\omega\tilde{\boldsymbol{u}}\to\frac{c_p}{\beta}[1-i\omega(\zeta-\mathcal{C})]\nabla\tilde{\Theta}_2+\eta\nabla\times\boldsymbol{k}\tilde{\Omega}, \tag{30}$$

$$\tilde{s}\to\tilde{p}\to\frac{c_p}{\beta}\left[\frac{1-i\omega(\zeta-\mathcal{C})}{1-i\omega\zeta}\right]\tilde{\Theta}_2. \tag{31}$$

Clearly as $\beta\to0$, $\tilde{\Theta}_2/\beta$ must remain bounded and $\tilde{\Theta}_2$ must vanish, if the physical variables $\tilde{\boldsymbol{u}}$, $\tilde{s}$ and $\tilde{p}$ are to remain finite, whence from Eq. (12), $\tilde{\theta}\to\tilde{\Theta}_1$. Finally, using Eq. (31) to eliminate $\tilde{\Theta}_2$ from Eq. (30), we see that

$$i\omega\tilde{\boldsymbol{u}}\to(1-i\omega\zeta)\nabla\tilde{p}+\eta\nabla\times\boldsymbol{k}\tilde{\Omega}, \tag{32}$$

which, if β is set to zero at the outset, follows directly from Eqs. (1), (2), the first of Eq. (4), and the definition of Ω [given just prior to Eq. (9)]. And we note that $\tilde{p}$ now satisfies

$$\left(\nabla^2+\frac{\omega^2}{1-i\omega\zeta}\right)\tilde{p}=0. \tag{33}$$

In this limit, the visco-acoustic and thermal problems appear to decouple completely, which of course cannot be the case because viscous *losses* in the former problem cause thermal heating of the fluid. This anomaly arises because non-linear terms associated with viscous stresses were neglected in the energy/heat equation [Eq. (3)]. In most circumstances, this is perfectly acceptable, but in the limit $\beta\to0$, these non-linear terms become the dominant source term of the heat equation. Thus, in the limit $\beta\to0$, the visco-acoustic problem can be solved without reference to thermal effects and the viscous stresses from its solution lead to known, non-linear, source terms in the thermal problem. We note, however, that if non-linear effects are significant in the energy equation, it may be necessary to revisit the form of the equations of state; see, for example, Pierce (1978).

IV. IMPLEMENTATION FOR AIR AND WATER FILLED CHANNELS

The theory is now implemented in the case of air and water filled channels. Relevant parameters are listed in Table I, taken from Dunn *et al.* (2015), and assumed independent of frequency.

In Sec. IV A, we evaluate the phase speed and attenuation of acoustic waves propagating along air-filled and water-filled channels, by finding the lowest order roots of the dispersion equations derived in Sec. III. The results are presented as a function of the channel width, $\bar{W}=2\bar{L}$, relative to Stokes's boundary layer thickness, $\bar{\delta}_s$, where the latter is defined by

$$\bar{\delta}_s=2\pi\sqrt{\frac{2\,\bar{\nu}}{\bar{\omega}}}, \tag{34}$$

and $\bar{\nu}$, the kinematic viscosity, is related to the dynamic viscosity, $\bar{\eta}$, through $\bar{\nu}=\bar{\eta}/\bar{\rho}_0$. The phase-speed values

TABLE I. Thermo-viscous parameter values for water and air, taken from Dunn *et al.* (2015), noting that $\bar{\beta} = 1/\bar{T}_0$ for an ideal gas.

Parameter	Unit	Symbol	Water (10 °C)	Air (27 °C)
Speed of sound	$\mathrm{m\,s^{-1}}$	$\bar{c}_0$	1490	343
Density	$\mathrm{kg\,m^{-3}}$	$\bar{\rho}_0$	1000	1.19
Dynamic shear viscosity	$\mathrm{kg\,m^{-1}\,s^{-1}}$	$\bar{\eta}$	1.002×10^{-3}	1.846×10^{-5}
Dynamic bulk viscosity	$\mathrm{kg\,m^{-1}\,s^{-1}}$	$\bar{\eta}_B$	3.006×10^{-3}	1.108×10^{-5}
Thermal conductivity	$\mathrm{W\,m^{-1}\,K^{-1}}$	$\bar{\mathcal{K}}$	0.597	2.624×10^{-2}
Specific heat at constant pressure	$\mathrm{J\,kg^{-1}\,K^{-1}}$	$\bar{c}_p$	4192	1005
Ambient temperature	K	$\bar{T}_0$	283.16	300
Coefficient of thermal expansion	$\mathrm{K^{-1}}$	$\bar{\beta}$	8.822×10^{-5}	1/300

obtained for an air-filled channel are compared with the experimental data of Ward *et al.* (2015), noting that these data are parameterized against $\bar{\delta}_\nu/\bar{W}$, rather than $\bar{\delta}_s/\bar{W}$, where

$$\bar{\delta}_\nu = \sqrt{\frac{\bar{\nu}}{\bar{\omega}}} \approx 0.11\bar{\delta}_s. \tag{35}$$

In Sec. IV B, we examine the fluid-particle-velocity profile across the channel for various channel widths in order to determine the extent to which the channel-wall boundary-layer influences the motion of the fluid and hence the propagation of acoustic waves.

A. Phase speed and attenuation

Given the root, k, for any one of the dispersion Eqs. (23), (25), and (27), the *complex* non-dimensionalized phase-speed, v, along the channel is given by

$$v = \frac{\bar{v}}{\bar{c}_0} = \frac{\omega}{k}. \tag{36}$$

Roots for the dispersion equations were calculated using the MATLAB [version 9.2.0.556344 (R2017a)] command *fsolve*, which finds the local zero of a user-specified function close to a given starting point.

Before presenting the results thereby obtained, we first note that in air and water both $\omega\zeta$ and $\omega\mathcal{C}$ are very much less than unity at frequencies up to the order of 1 GHz. Under these circumstances, and provided $\omega \ll 1$, the following approximate expressions for the (dimensionless) complex phase-speed can be obtained from Eqs. (23) and (25):

$$v_{insul} \approx \sqrt{1 - \tanh\left(\frac{1-i}{\sqrt{2}\,\delta_\nu}\right) \Big/ \left(\frac{1-i}{\sqrt{2}\,\delta_\nu}\right)} \tag{37}$$

and

$$v_{cond} \approx \sqrt{\frac{1 - \tanh\left(\frac{1-i}{\sqrt{2}\,\delta_\nu}\right) \Big/ \left(\frac{1-i}{\sqrt{2}\,\delta_\nu}\right)}{1 + \frac{\mathcal{A}-1}{\sqrt{\mathrm{Pr}}} \tanh\left(\frac{1-i}{\sqrt{2}\,\delta_\theta}\right) \Big/ \left(\frac{1-i}{\sqrt{2}\,\delta_\nu}\right)}}, \tag{38}$$

where $\delta_\nu = \bar{\delta}_\nu/\bar{L}$ is Ward's (Ward *et al.*, 2015) viscous boundary layer parameter, non-dimensionalized on the half-width $\bar{L}$ of the duct; $\delta_\theta = \bar{\delta}_\theta/\bar{L}$ is an equivalent thermal boundary layer parameter with $\bar{\delta}_\theta$ defined as

$$\bar{\delta}_\theta = \sqrt{\frac{\bar{\mathcal{K}}}{\bar{\rho}_0\bar{\omega}\bar{c}_p}}; \tag{39}$$

and Pr is the Prandtl number, which is given by

$$\mathrm{Pr} = \frac{\bar{\eta}\bar{c}_p}{\bar{\mathcal{K}}} = \left(\frac{\bar{\delta}_\nu}{\bar{\delta}_\theta}\right)^2. \tag{40}$$

The expression for v_{insul} is independent of all thermal parameters and varies only with the dimensionless parameter $\bar{L}/\bar{\delta}_\nu$. However, v_{cond} is additionally dependent upon Pr and the dimensionless parameter $\mathcal{A} - 1 = (\bar{\beta}^2\bar{T}_0\bar{c}_0^2)/\bar{c}_p$, noting that Eq. (38) recovers Stinson's solution for an ideal gas (Stinson, 1991) if $\mathcal{A}$ is replaced by the ratio of specific heats at constant pressure and volume.

If the fundamental thermo-viscous parameters are frequency independent, as assumed here, we see that in the cases of thermally insulating and perfectly conducting channel-wall boundary conditions, the functional frequency dependence of their associated complex phase-speeds is contained entirely within the expressions for the boundary layer parameters $\bar{\delta}_\nu$ and $\bar{\delta}_\theta$. Indeed, given the definition in Eq. (40) of Pr, it is sufficient to specify just one of the boundary layer parameters and the Prandtl number, which is frequency independent.

Although not illustrated herein, we find that for the range of channel-widths under consideration, Eqs. (37) and (38) are in almost exact agreement with values obtained using the full dispersion equations at all frequencies up to at least 1 MHz in air and 50 MHz in water. Furthermore, their validity is not confined to air and water. Indeed, these expressions are valid for any Newtonian fluid, provided the conditions specified in their derivation are satisfied, namely, $\omega\zeta \ll 1$, $\omega\mathcal{C} \ll 1$, and $\omega \ll 1$.

Returning to the solutions of the exact dispersion equations, we note from Eqs. (37) and (38) that as $\bar{L}, \bar{W} \to \infty$, both v_{insul} and v_{cond} tend to unity, which is equivalent to $k \to \omega$. Thus, an appropriate method for finding their roots, using *fsolve*, is to begin with a wide channel (we chose $\bar{W} = 100\bar{\delta}_s$), and to start the root search from $k = \omega$. We then gradually reduce $\bar{W}$ down to the desired value, using the root found for the previous (larger) value of $\bar{W}$ as a new starting point for *fsolve*.

By way of example, Fig. 2 shows the resulting *real* phase-speed and attenuation along an air-filled channel as a function of $\bar{\delta}_s/\bar{W}$. Here, real phase-speed is defined as $\Re(v)$, and the attenuation in dB/wavelength is $40\pi(k_i/k_r)\log_{10}(e)$, where $k_r = \Re(k)$ and $k_i = \Im(k)$. The curves for viscous only and thermally insulating channel-wall boundary conditions are identical, indicating that for a thermally insulating boundary condition, the lowest order symmetric duct mode is decoupled from thermal fluctuations as expected. However, a different behavior is observed for the conducting curve shown in Fig. 2, again as expected. We observe that the results of Ward *et al.* (2015), indicted by the black crosses of Fig. 2, lie in-between the two extreme thermal boundary conditions of conducting and insulating channel walls. Although not presented here, we find that the behavior in air, illustrated in Fig. 2, is valid at all frequencies up to the order of 1 MHz.

Figure 3 demonstrates the behavior of a water-filled channel, which is found to be valid at all frequencies below a maximum value approaching 50 MHz. The behavior of water is very similar to that of air, except that for water, thermal effects are seen to be negligible for both the thermally conducting (isothermal) and insulating channel-wall boundary conditions, primarily because of water's low coefficient of thermal expansion (as discussed previously). For water this leads to the parameter $\mathcal{A}$ being very close to unity, $\mathcal{A} \approx 1.001$ in water, whilst in air $\mathcal{A} \approx 1.39$. In addition, Pr in water is about ten times greater than in air. Taken together, these two factors lead to the second term in the denominator of Eq. (38) being negligible for water, thereby recovering Eq. (37).

In summary, we see that in water, thermal effects have a negligible impact upon acoustic propagation along narrow channels, and this is also true in air if the channel wall is

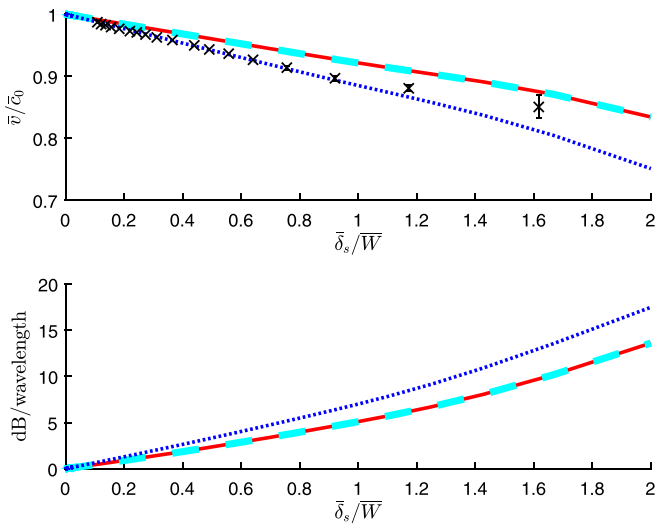

FIG. 2. (Color online) Phase speed and attenuation along an air-filled channel. The upper plot shows the phase speed relative to $\bar{c}_0$. The lower plot shows the attenuation along the channel. Different line styles indicate channel-wall boundary conditions corresponding to Viscous only (red, solid); Thermally insulating (cyan, dashed); Isothermal/conducting (blue, dotted). The black crosses indicate the *single slit* measured data extracted from Fig. 4 of Ward *et al.* (2015), and reproduced here by kind permission of Professor Alastair Hibbins.

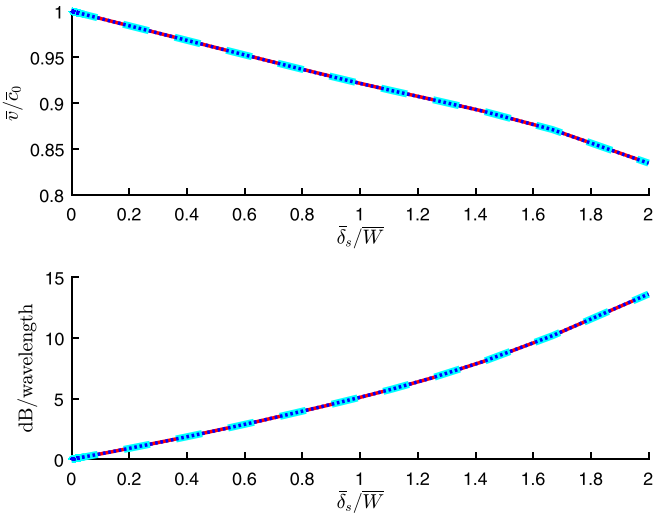

FIG. 3. (Color online) Phase speed and attenuation along a water-filled channel. The upper plot shows the phase speed relative to $\bar{c}_0$. The lower plot shows the attenuation along the channel. Line styles are as indicated in Fig. 2.

thermally insulating, which is perhaps not surprising as this boundary condition is close to the adiabatic thermal condition expected in freely propagating acoustic waves. However, in air, thermal effects are significant when the channel wall is conducting. For the thermally insulating channel wall boundary condition, the behavior of air and water with respect to their dimensionless phase speed and attenuation along the channel in dB/wavelength is essentially identical when parameterized against the dimensionless parameter $\bar{\delta}_s/\bar{W}$. Note, however, that the attenuation along a fixed distance, say 1 m, is much less in water than in air due to the higher dimensional phase speed of water, leading to a wavelength in water that is about five times greater than in air. As an example in this case of rigid boundaries where the channel width is of the order of the boundary layer thickness, the attenuation in air at 10 kHz can be over 200 dB m^{-1}, whereas in water it is less than 37 dB m^{-1}.

B. Fluid particle velocity profiles

Similar behavior to that discussed above is observed for the fluid particle velocity profiles across the channel. Below, we plot the x- and y-components of fluid particle velocity, normalized so that $u_x(y=0)=1$. For fluids such as air and water, which are characterized by low viscous and diffusion coefficients, we find that for both the insulating and isothermal channel-wall boundary conditions, $u_x(y)/u_x(0)$ depends only upon the non-dimensionalized viscous boundary layer parameter $\delta_\nu = \bar{\delta}_\nu/\bar{L}$; *there is no dependence upon the thermal properties of the fluid*. For air, this is illustrated in the upper plot of Fig. 4 for a channel-width of $10\bar{\delta}_s$. Both the magnitude and the phase (the latter is not shown) of $u_x(y)/u_x(0)$ have the same values for all three channel wall boundary conditions. The same behavior (not shown) is observed in water.

For the y-component of fluid-particle velocity, we find that in the case of a thermally insulating channel-wall, the scaled parameter $u_y(y)/(\eta\, u_x(0))$ depends upon only δ_ν. However, when the channel wall is perfectly conducting,

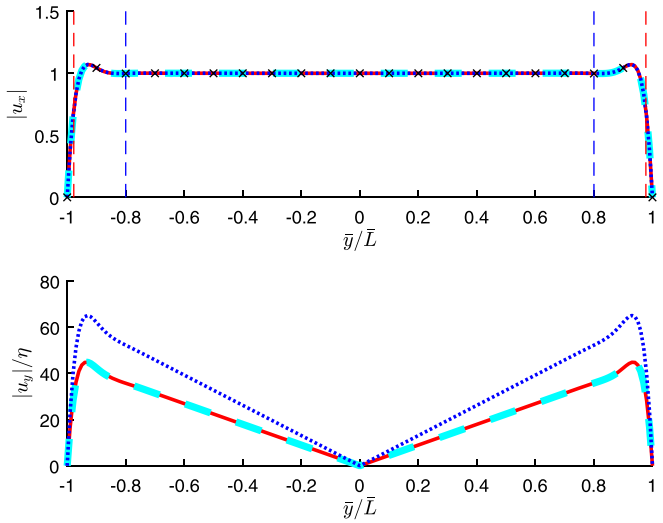

FIG. 4. (Color online) Magnitude of the fluid particle velocity across an air-filled channel of width of 10 $\bar{\delta}_s$. The upper plot shows the x-component of the fluid particle velocity, and the lower plot shows the y-component; $\boldsymbol{u}$ is normalized, independently for each boundary condition, such that $u_x(y=0)=1$. Line styles are as indicated in Fig. 2. On the upper plot: the black crosses indicate Stokes solution for a fluid half-space; the blue-dashed vertical lines indicate the position of Stokes's boundary layer thickness, $\bar{\delta}_s/\bar{L}$, relative to the channel walls at $y=\pm1$; the red-dashed vertical lines indicate the location of $\bar{\delta}_\nu/\bar{L}$.

$u_y(y)/(\eta\, u_x(0))$ depends, in general, also upon the additional parameters $\delta_\theta=\bar{\delta}_\theta/\bar{L}$ and $\mathcal{A}-1=\beta^2/c_p$, or alternatively its behavior may be characterized in terms of δ_ν, the Prandtl number Pr, and β^2/c_p. For air, this behavior is illustrated in the lower plot of Fig. 4 for a channel-width of $10\bar{\delta}_s$. We see that whilst the viscous only and thermally insulating velocity profiles are identical, the profile for a conducting wall is different, demonstrating the influence of thermal effects in this case. Although not shown here, in water, the three thermal boundary conditions have identical velocity profiles as a result of water's low coefficient of expansion.

In the absence of boundary layer effects, the y-component of fluid particle velocity would be zero everywhere, and the x-component would be constant across the channel; that is u_x would be independent of y. The red and blue, vertical, dashed lines marked on the upper plot of Fig. 4 indicate, respectively, the positions of the non-dimensionalized boundary layer thickness parameters, $\bar{\delta}_\nu/\bar{L}$ and $\bar{\delta}_s/\bar{L}$, relative to the channel walls on $y=\pm1$. The black crosses show Stokes's solution for an oscillating pressure gradient within a fluid-filled half-space lying above a rigid surface, under the assumption that the boundary layers on the two walls of the channel are well separated and hence non-interacting (Batchelor, 2000). For this relatively wide channel, the fluid-particle-velocity profile for u_x is very similar to that of Stokes's half-space solution, and we observe that $\bar{\delta}_s$ is a significantly better indicator than $\bar{\delta}_\nu$, of the extent to which the channel-wall boundary layers disturb the motion of the fluid. $\bar{\delta}_\nu$ underestimates the true extent of the boundary layer but as we have seen above it is a very useful parameter with which to characterize the fluid's behavior when it is influenced by boundary layer effects.

Figure 5 shows the velocity profile for a much narrower channel, $\bar{W}=\bar{\delta}_s/2$, in which the boundary layers on the two walls are strongly interacting. Stokes's solution for a fluid half-space is no longer relevant; rather the velocity profile resembles that of Poiseuille flow, as indicated by the red crosses. Using $\bar{\delta}_\nu/\bar{L}$ as boundary layer thickness can be seen in Fig. 5 to be severely underestimating this length.

The large difference in the magnitude of the y-component of fluid particle velocity, which is observed in Figs. 4 and 5, arises mainly because the expression for $u_y(y)/(\eta\, u_x(0))$ contains a scaling factor of $1/\delta_\nu$.

V. FLUID-STRUCTURE INTERACTION EFFECTS

Until now, all boundaries have been considered rigid, which is a sensible approximation in the air-filled channel but not necessarily so in the case of a water-filled channel. In order to investigate the effect of elastic boundaries, and in particular their impact upon phase-speed and attenuation in this case, let us consider a water-filled channel in an undamped elastic medium of infinite extent; the only damping mechanism considered is the viscosity of the fluid. The presence of semi-infinite elastic walls requires the consideration of body waves, both compressional and shear, propagating within the elastic material. Generally, this necessitates the mathematical formulation of a physical problem with some specified forcing, the solution of which will be expressed in terms of integrals around branch-cuts that are then associated with outgoing and incoming body waves and additionally, a sum of the natural modes of propagation in the waveguide. However, such an analysis is beyond the scope of the present study; we are primarily concerned with demonstrating the impact of an elastic boundary on the natural modes of propagation within the water-filled channel, and comparing this behavior to the idealized case of a rigid boundary. In order to proceed here then we must

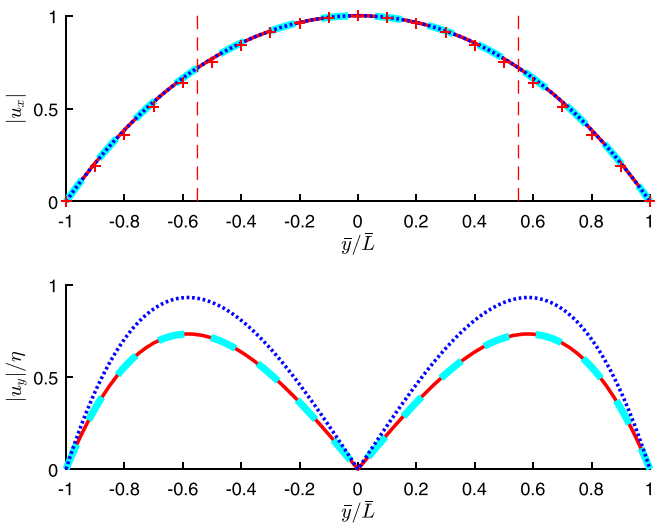

FIG. 5. (Color online) Magnitude of the fluid particle velocity across an air-filled channel of width of $\bar{\delta}_s/2$. The upper plot shows the x-component of fluid-particle-velocity, and the lower plot shows the y-component; $\boldsymbol{u}$ is normalized, independently for each boundary condition, such that $u_x(y=0)=1$. Line styles are as indicated in Fig. 2. On the upper plot: the red crosses indicate the velocity profile for Poiseuille flow across a narrow channel, the red-dashed vertical lines indicate the location of $\bar{\delta}_\nu/\bar{L}$.

merely ensure that the choice of branch cuts is consistent with the requirements of causality. This is discussed further below.

We shall neglect all thermal effects in this analysis since as shown earlier these are negligible in the case of acoustic propagation in water (due to the low value of the thermal expansion coefficient). Recalling that as $\beta \to 0$, $s \to p$, the (time-harmonic) fluid velocity here is therefore written compactly in terms of the condensation and vorticity, i.e.,

$$\tilde{\mathbf{u}} = \frac{-i}{\omega}\left((1 - i\omega\zeta)\nabla\tilde{s} + \eta\nabla \times \tilde{\Omega}\right), \tag{41}$$

where $\tilde{s}$ is governed by

$$\left(\nabla^2 + \frac{\omega^2}{1 - i\omega\zeta}\right)\tilde{s} = 0. \tag{42}$$

The components of the *total* (time-harmonic) fluid stress tensor are

$$\tilde{\Sigma}_{ij} = \tilde{\sigma}_{ij} - \tilde{p}\delta_{ij} = \eta\left(\frac{\partial\tilde{u}_i}{\partial x_j} + \frac{\partial\tilde{u}_j}{\partial x_i}\right) - \delta_{ij}(1 - i\omega\eta')\tilde{s}. \tag{43}$$

Next, referring back to Fig. 1, instead of imposing the rigid no-slip conditions [Eq. (19)] on the boundary, we now suppose that the medium in $|y| \geq 1$ is a linear isotropic elastic medium of infinite extent. Using a consistent non-dimensionalization scheme to that defined for the fluid with time-harmonic dependence $e^{-i\omega t}$, Navier's equations of linear elasticity may be written as

$$(\lambda + 2\mu)\nabla\tilde{\phi} - \mu\nabla \times \tilde{\boldsymbol{\psi}} + \omega^2\rho_s\tilde{\boldsymbol{w}} = 0, \tag{44}$$

where λ is the Lamé modulus and μ the shear modulus, both being non-dimensionalized on $\bar{\rho}_0\bar{c}_0^2$. Furthermore, $\rho_s = \bar{\rho}_s/\bar{\rho}_0$ denotes the non-dimensionalized solid density and $\boldsymbol{w} = (w_x, w_y, 0) = \bar{\boldsymbol{w}}/\bar{L}$ is the non-dimensionalized elastic displacement, with a tilde denoting its time-harmonic counterpart. Furthermore, the following potentials have been introduced, $\tilde{\phi} = \nabla \cdot \tilde{\boldsymbol{w}}$, and $\tilde{\boldsymbol{\psi}} = \nabla \times \tilde{\boldsymbol{w}}$. As with the fluid vorticity, the rotation vector $\tilde{\boldsymbol{\psi}}$ points in the z-direction and may be written $\tilde{\boldsymbol{\psi}} = \hat{\boldsymbol{k}}\tilde{\psi}$. The scalar potentials $\tilde{\phi}$ and $\tilde{\psi}$ satisfy the Helmholtz equations

$$(\nabla^2 + \kappa_p^2)\tilde{\phi} = 0, \tag{45}$$

$$(\nabla^2 + \kappa_s^2)\tilde{\psi} = 0, \tag{46}$$

where κ_p and κ_s are the non-dimensionalized compressional and shear wavenumbers

$$\kappa_p = \omega\sqrt{\frac{\rho_s}{\lambda + 2\mu}} = \bar{\omega}\bar{L}\sqrt{\frac{\bar{\rho}_s}{\bar{\lambda} + 2\bar{\mu}}},$$
$$\kappa_s = \omega\sqrt{\frac{\rho_s}{\mu}} = \bar{\omega}\bar{L}\sqrt{\frac{\bar{\rho}_s}{\bar{\mu}}}. \tag{47}$$

The elastic displacement is written simply using Eq. (44) in the form

$$\tilde{\boldsymbol{w}} = -\frac{1}{\omega^2\rho_s}\left[(\lambda + 2\mu)\nabla\tilde{\phi} - \mu\nabla \times \tilde{\boldsymbol{\psi}}\right], \tag{48}$$

which is the analogous form, in terms of potentials, to the fluid velocity expression in Eq. (41). Finally, the (time-harmonic) elastic stress tensor is given by

$$\tilde{\sigma}_{ij} = \delta_{ij}\lambda\tilde{\phi} + \mu\left(\frac{\partial\tilde{w}_i}{\partial x_j} + \frac{\partial\tilde{w}_j}{\partial x_i}\right). \tag{49}$$

As with the case of a rigid-walled channel, we seek solutions in k-space, which again we denote by the $\hat{}$ symbol. For the fluid-structure interaction problem, it is convenient to relate the x- and k-space potentials of the elastic solid as follows:

$$\tilde{\phi}(x, y, w) = \frac{\rho_s}{\lambda + 2\mu}\,\hat{\phi}(k, y, w)e^{ikx},$$
$$\tilde{\psi}(x, y, w) = \frac{\rho_s}{\mu}\,\hat{\psi}(k, y, w)e^{ikx}, \tag{50}$$

with $\hat{\phi}$ and $\hat{\psi}$ satisfying

$$\left(\frac{\partial^2}{\partial y^2} - \gamma_p^2\right)\hat{\phi} = 0, \quad \left(\frac{\partial^2}{\partial y^2} - \gamma_s^2\right)\hat{\psi} = 0, \tag{51}$$

where

$$\gamma_p = (k^2 - \kappa_p^2)^{1/2}, \quad \gamma_s = (k^2 - \kappa_s^2)^{1/2}. \tag{52}$$

The choice of cuts for γ_p and γ_s are discussed shortly. For the fluid, we write

$$\tilde{s}(x, y, w) = \frac{1}{1 - i\omega\zeta}\hat{s}(k, y, w)e^{ikx},$$
$$\tilde{\Omega}(x, y, w) = \frac{1}{\eta}\hat{\Omega}(k, y, w)e^{ikx}, \tag{53}$$

with $\hat{s}$ and $\hat{\Omega}$ satisfying

$$\left(\frac{\partial^2}{\partial y^2} - \gamma_2^2\right)\hat{s} = 0, \quad \left(\frac{\partial^2}{\partial y^2} - \alpha^2\right)\hat{\Omega} = 0, \tag{54}$$

where $\gamma_2 = (k^2 - \omega^2/(1 - i\omega\zeta))^{1/2}$ and we recall that $\alpha = (k^2 - i\omega/\eta)^{1/2}$.

A. The boundary value problem

Boundary conditions require continuity of displacement/velocity at the fluid-solid interface and continuity of the traction components across the channel wall. In k-space, these conditions require, for the velocity

$$\frac{\partial\hat{\boldsymbol{w}}}{\partial t}(k, y = \pm 1) = -i\omega\hat{\boldsymbol{w}}(k, y = \pm 1) = \hat{\boldsymbol{u}}(k, y = \pm 1); \tag{55}$$

and for the traction

$$\hat{\sigma}_{yy}(k,y=\pm1)=\hat{\Sigma}_{yy}(k,y=\pm1), \tag{56}$$

$$\hat{\sigma}_{xy}(k,y=\pm1)=\hat{\Sigma}_{xy}(k,y=\pm1), \tag{57}$$

noting that $\tilde{\boldsymbol{w}}(x,y,\omega)=\hat{\boldsymbol{w}}(k,y,\omega)e^{ikx}$, $\tilde{\boldsymbol{u}}(x,y,\omega)=\hat{\boldsymbol{u}}(k,y,\omega)e^{ikx}$ and similarly for the stress components.

By inserting Eqs. (50) and (53) into Eqs. (41), (43), (48), and (49), as appropriate, and imposing the boundary conditions from Eqs. (55)–(57), we obtain the following constraints upon our solutions at $y=\pm1$:

$$\boldsymbol{\nabla}\hat{s}+\boldsymbol{\nabla}\times\hat{\Omega}=-\left[\boldsymbol{\nabla}\hat{\phi}-\boldsymbol{\nabla}\times\hat{\psi}\right], \tag{58}$$

$$\left(\frac{\omega^2}{\mu}+2ik^2\mathcal{P}\right)\hat{s}+2k\mathcal{P}\frac{\partial\hat{\Omega}}{\partial y}=\left(2k^2-\kappa_s^2\right)\hat{\phi}+2ik\frac{\partial\hat{\psi}}{\partial y}, \tag{59}$$

$$2k\mathcal{P}\frac{\partial\hat{s}}{\partial y}-\left(\frac{\omega^2}{\mu}+2ik^2\mathcal{P}\right)\hat{\Omega}=-2ik\frac{\partial\hat{\phi}}{\partial y}+\left(2k^2-\kappa_s^2\right)\hat{\psi}, \tag{60}$$

where

$$\mathcal{P}=\left(\frac{\omega\eta}{\mu}\right)=\left(\frac{\bar{\omega}\bar{\eta}}{\bar{\mu}}\right). \tag{61}$$

Note that $\omega^2/\mu(=\kappa_s^2/\rho_s=\bar{\rho}_0\bar{\omega}^2\bar{L}^2/\bar{\mu})$ and $\mathcal{P}$ are measures of the fluid loading acting on the elastic wall, i.e., they are measures of the fluid's inertial and viscous forces relative to the elastic stresses at the channel-wall. Clearly they are important non-dimensional parameters that will influence significantly the characteristics of our solution, although we note below that in the air and water cases, as well as a wide range of other scenarios $\mathcal{P}\ll1$ and can be set to zero in order to simplify the dispersion relation. Other important non-dimensional parameters (most of which have been defined previously) include

$$\mu=\frac{\bar{\mu}}{\bar{\rho}_0\bar{c}_0^2},\quad \eta=\frac{\bar{\eta}}{\bar{\rho}_0\bar{c}_0\bar{L}},\quad \rho_s=\frac{\bar{\rho}_s}{\bar{\rho}_0},\quad \epsilon=\frac{\bar{\eta}'}{\bar{\eta}},\quad \delta_\nu=\sqrt{\frac{\eta}{\omega}}. \tag{62}$$

With these definitions, the other non-dimensional parameters that arise can be written as

$$\kappa_s=\omega\sqrt{\frac{\rho_s}{\mu}},\quad \kappa_p=\kappa_s\sqrt{\frac{1-2\upsilon}{2(1-\upsilon)}},\quad \omega\zeta=(2+\epsilon)\mu\mathcal{P}, \tag{63}$$

where υ denotes Poisson's ratio.

B. Dispersion relations for symmetric modes in a fluid-filled channel within an infinite elastic solid

As for the rigid-walled channel, only modes where s is symmetric in y are considered here. In this problem (that is independent of thermal effects), the k-space vorticity and condensation then take the form

$$\hat{\Omega}=E\sinh(\alpha y),\quad \hat{s}=F\cosh(\gamma_2 y). \tag{64}$$

For the solid, appropriate symmetric solutions to Eqs. (51) and (52) are similarly given by

$$\hat{\phi}(k,y\geq1)=Xe^{-\gamma_p(y-1)},\quad \hat{\phi}(k,y\leq-1)=Xe^{\gamma_p(y+1)}, \tag{65}$$

$$\hat{\psi}(k,y\geq1)=Ye^{-\gamma_s(y-1)},\quad \hat{\psi}(k,y\leq-1)=-Ye^{\gamma_s(y+1)}, \tag{66}$$

in which the square root functions of Eq. (52) are chosen such that $\gamma_p\to k$ and $\gamma_s\to k$ as $k\to\infty$, with the branch cuts from κ_p and κ_s taken in the upper-half plane and those from $-\kappa_p$ and $-\kappa_s$ taken in the lower-half plane. To be definitive in the calculations below, the branch cuts are chosen to run parallel to the imaginary axis from their respective branch points.

The dispersion equation in k for the natural modes of propagation is obtained by substituting the solution forms from Eqs. (64)–(66) into the boundary conditions from Eqs. (58)–(60), evaluated on $y=\pm1$. Requiring the determinant of the resulting set of simultaneous equations, in the unknown coefficients E, F, X, and Y, to be zero then leads to the following dispersion equation:

$$\begin{aligned}\mathcal{D}_{ve}=\frac{1}{\mathcal{D}_1\mathcal{D}_2}\Bigg\{&\mathcal{D}_{vr}\left\{\mathcal{D}_1+4ik^2\mathcal{P}\left[\mathcal{D}_2(2+i\mathcal{P})-\kappa_s^2\right]\right\}\\&+\frac{\kappa_s^2}{\rho_s}\Big\{2k^2\left[2\mathcal{D}_2(1+i\mathcal{P})-\kappa_s^2\right]\\&\times\tanh\alpha-\kappa_s^2\left[\alpha\gamma_p+\gamma_s\gamma_2\tanh\gamma_2\tanh\alpha\right]\Big\}\\&+\frac{\kappa_s^4}{\rho_s^2}\mathcal{D}_2\tanh\alpha\Bigg\}=0,\end{aligned} \tag{67}$$

where $\mathcal{D}_1=(2k^2-\kappa_s^2)^2-4k^2\gamma_s\gamma_p=0$ is Rayleigh's dispersion equation for natural modes on the surface of a stress-free elastic half-space, and $\mathcal{D}_2=k^2-\gamma_s\gamma_p$ is the dispersion equation for the natural modes on the surface of a clamped elastic half-space. Furthermore, $\mathcal{D}_{vr}$ is the dispersion equation [Eq. (27)] for the natural modes of propagation along a rigid-walled channel filled with a viscous fluid in which thermal effects are negligible. We note that in the limit of $\mu,\rho_s\to\infty$ with $\mu/\rho_s=$ constant, Eq. (67) reduces to $\mathcal{D}_{vr}=0$.

C. Fluid structure interaction implementation for air and water filled channels in steel

Let us now consider the implementation of the above in the specific case of a fluid-filled channel in steel with density $\bar{\rho}_s=7871\ \mathrm{kg\ m^{-3}}$, and compressional and shear wave-speed $\bar{v}_p=6000\ \mathrm{m\ s^{-1}}$ and $\bar{v}_s=3000\ \mathrm{m\ s^{-1}}$, respectively. These parameter values imply a shear modulus $\bar{\mu}=70.839$ GPa and a Lamé modulus $\bar{\lambda}=141.68$ GPa.

For air- and water-filled channels, $\mathcal{P}\ll1$ and may be set to zero in Eq. (67). Furthermore, as discussed in Sec. IV A, at frequencies and channel-widths of interest $\omega\zeta\ll1$, $\omega\ll1$, and we expect $k=O(\omega)$. Thus, $\alpha\approx\sqrt{-i\omega/\eta}=(1-i)/\sqrt{2}\delta_\nu$, which is independent of k, and $\gamma_2\approx\sqrt{k^2-\omega^2}$, where $|\gamma_2|\ll1$. Under these conditions, we find that the non-dimensional phase speed, $v=\omega/k$, satisfies the following approximate dispersion equation:

$$\mathcal{D}_{ve} \approx \frac{1}{\hat{\mathcal{D}}_1\hat{\mathcal{D}}_2}\left\{\hat{\mathcal{D}}_1\left[\frac{\tanh\alpha}{\alpha}-(1-v^2)\right]\right.$$
$$+\frac{1}{\rho_s}\frac{v^2}{v_s^2}\left\{2\left[2\hat{\mathcal{D}}_2-\frac{v^2}{v_s^2}\right]\frac{\tanh\alpha}{\alpha}\right.$$
$$\left.-\frac{v^2}{v_s^2}\left[\frac{v}{\omega}\hat{\gamma}_p+\frac{\omega}{v}\hat{\gamma}_s(1-v^2)\frac{\tanh\alpha}{\alpha}\right]\right\}$$
$$\left.+\frac{1}{\rho_s^2}\frac{v^4}{v_s^4}\hat{\mathcal{D}}_2\frac{\tanh\alpha}{\alpha}\right\}=0, \tag{68}$$

where $\hat{\gamma}_p=\sqrt{1-v^2/v_p^2}$, $\hat{\gamma}_s=\sqrt{1-v^2/v_s^2}$, $\hat{\mathcal{D}}_1=(2-v^2/v_s^2)^2-4\hat{\gamma}_s\hat{\gamma}_p$, $\hat{\mathcal{D}}_2=1-\hat{\gamma}_s\hat{\gamma}_p$, with $v_p=\bar{v}_p/\bar{c}_0$ and $v_s=\bar{v}_s/\bar{c}_0$ being the non-dimensional compressional and shear wave-speeds; all of these parameters are independent of frequency.

It is clear from the above expression that the dependence of phase speed upon frequency is somewhat more complicated for an elastic-walled channel than it is for the case of a rigid-walled channel, expressions for which are provided in Eqs. (37) and (38).

1. Phase speed and attenuation

All the results presented in this section were obtained from the full dispersion equation [Eq. (67)]. Figure 6 shows results for phase speed and attenuation as a function of $\bar{\delta}_s/\bar{W}$ along an air-filled channel in steel at 10 kHz, compared with those for a rigid-walled channel, noting that thermal effects have been neglected. Figure 7 reveals the behavior of a water-filled channel. Also illustrated in the latter are the phase speed and attenuation along a steel-walled channel neglecting viscosity. The latter data were obtained from the roots of the dispersion equation for an elastic-walled channel, filled with an inviscid fluid; these are derived from the boundary conditions applicable to this case, namely,

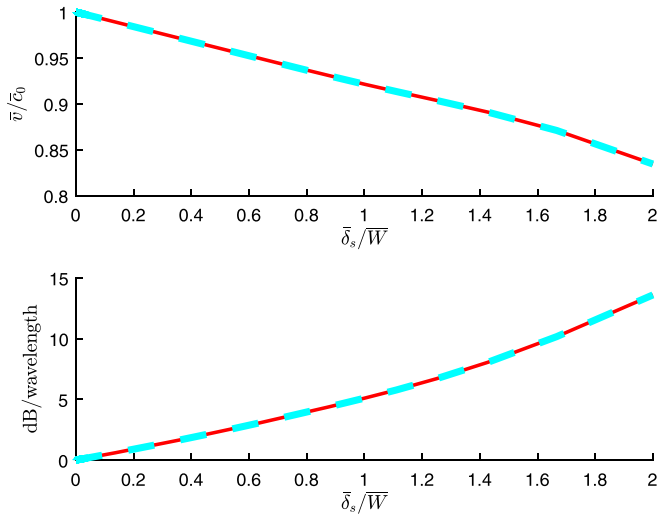

FIG. 6. (Color online) Phase speed and attenuation along an air-filled channel at 10 kHz. The upper plot shows the phase speed relative to $\bar{c}_0$. The lower plot shows the attenuation along the channel (dB/wavelength). In both plots, the solid red curve indicates a rigid-walled channel, and the dashed cyan curve is associated with a steel-walled channel. Thermal effects are neglected.

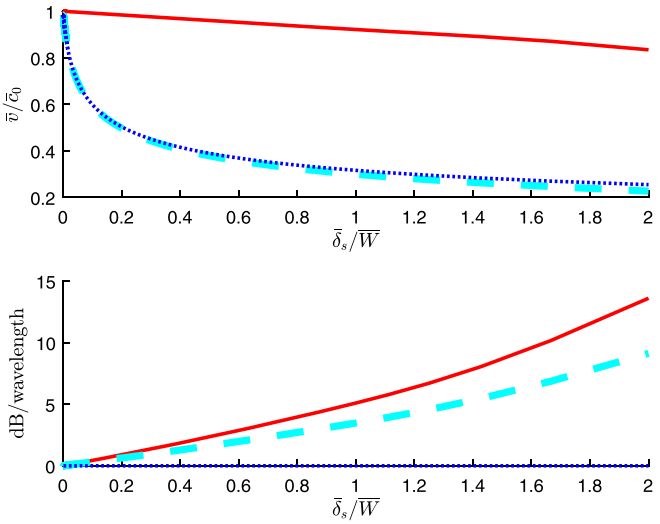

FIG. 7. (Color online) Phase speed and attenuation along a water-filled channel at 10 kHz. The upper plot shows the phase speed relative to $\bar{c}_0$. The lower plot shows the attenuation along the channel (dB/wavelength). In both plots, the solid red curve indicates results for a water-filled rigid-walled channel; the dashed cyan curve is associated with a water-filled steel-walled channel. The dotted blue curve is associated with propagation in a steel-walled water-filled channel where fluid viscosity is neglected. In all three cases, thermal effects are neglected.

$$\hat{\sigma}_{yy}(k,y=\pm1)=\hat{\Sigma}_{yy}(k,y=\pm1), \tag{69}$$
$$\hat{\sigma}_{xy}(k,y=\pm1)=0, \tag{70}$$
$$-i\omega\hat{w}_y(k,y=\pm1)=\hat{u}_y(k,y=\pm1), \tag{71}$$

in which viscosity is excluded by setting $E=\eta=\eta_B=0$. The dispersion equation, $\mathcal{D}_{ie}(\omega,k)=0$, is then readily shown to be

$$\mathcal{D}_{ie}(\omega,k)=\rho_s\gamma_2\tanh(\gamma_2)\left[(2k^2-\kappa_s^2)^2-4k^2\gamma_s\gamma_p\right]$$
$$+\kappa_s^4\gamma_p=0, \tag{72}$$

noting that if $\tanh(\gamma_2)$ were set to unity, Eq. (72) recovers the dispersion equation for Scholte waves, i.e., the dispersion equation for surface waves at the interface between elastic and fluid half spaces (Rauch, 1980).

It is clear from Fig. 6 that for air, the natural-mode behavior of the steel-walled channel is essentially indistinguishable from that of a rigid-walled channel when thermal effects are neglected, whereas in the case of a water-filled channel, these behaviors are dramatically different as seen in Fig. 7. This is due to the strong interaction between water and the steel wall, which has the effect of slowing down the phase speed of the natural mode and reducing its attenuation along the channel in terms of dB/wavelength. The damping mechanism for the mode is still that of dissipation within the viscous boundary layer on the steel wall, as opposed to radiation loss through the wall into the elastic material. This is apparent from the inviscid curves of Fig. 7, which show that fluid structure interaction is the main cause of the dramatic reduction in phase speed, but alone this mechanism gives no damping.

Although the attenuation in terms of dB/wavelength is substantially smaller in water for the steel-walled channel

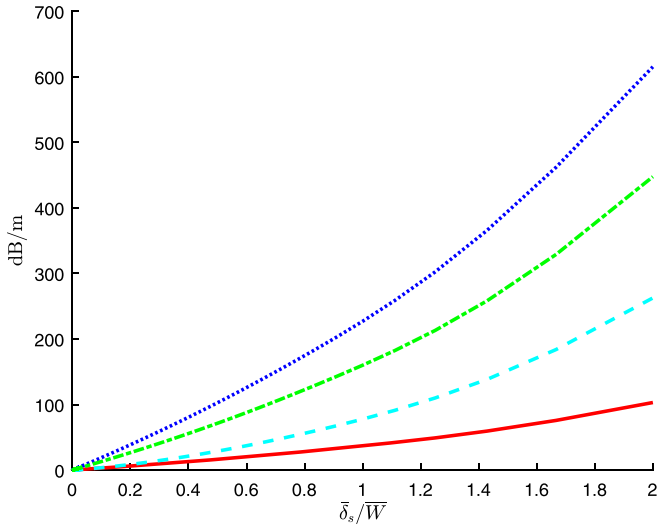

FIG. 8. (Color online) Attenuation along air and water-filled channels at 10 kHz (dB m^{-1}). Line styles indicate attenuation associated with propagation in a water-filled rigid-walled channel (solid red); a water-filled steel-walled channel (dashed cyan); an air-filled rigid-walled channel with isothermal boundary conditions (dotted blue); an air-filled rigid-walled channel with insulating boundary conditions (dash-dotted green).

than the rigid-walled case, the attenuation measured along a fixed length of say 1 m is actually greatly increased due to the large reduction in phase speed, which gives rise to a much smaller wavelength. This is illustrated in Fig. 8, which compares the attenuation at 10 kHz in dB m^{-1} along water-filled rigid and elastic walled channels. For comparison, the attenuation along an air-filled channel is also shown. We see that taken together, fluid-structure interaction and viscosity lead to a large increase in attenuation for the water-filled channel.

For completeness, Fig. 9 shows the behavior of a water-filled steel-walled channel at 100 kHz. Unlike the rigid-walled results discussed earlier, we see by comparison with Fig. 7

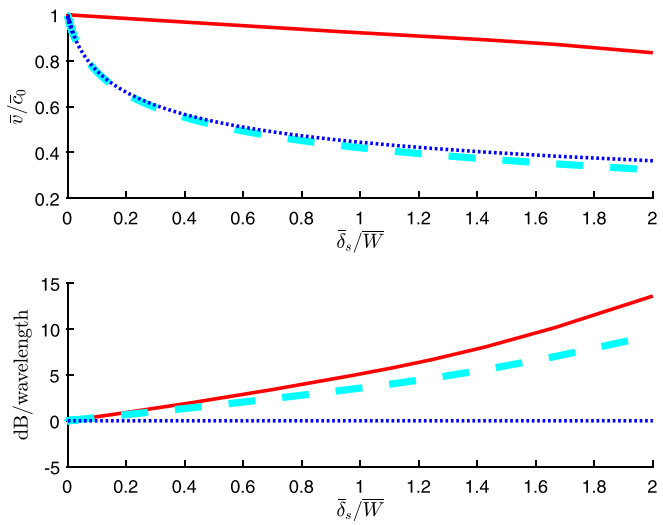

FIG. 9. (Color online) Phase speed and attenuation along a water-filled channel at 100 kHz. The upper plot shows the phase speed relative to $\bar{c}_0$. The lower plot shows the attenuation along the channel (dB/wavelength). In both plots, the solid red curve indicates results for a water-filled rigid-walled channel; the dashed cyan curve is associated with a water-filled steel-walled channel. The dotted blue curve is associated with propagation in a steel-walled water-filled channel, where fluid viscosity is neglected. In all three cases, thermal effects are neglected.

that the steel walled channel shows an additional frequency dependence beyond that associated with the thickness of the viscous boundary layer. This characteristic is illustrated further in Fig. 10, which illustrates the variation in phase speed and attenuation against non-dimensional frequency at a fixed value of $\bar{\delta}_s/\bar{W} = 1$. Whilst the attenuation is fairly constant across the range of values shown for ω, the variation in phase speed is considerable unlike the case of a rigid channel wall for which both parameters would be constant.

2. Particle velocity profiles

Figures 11 and 12 compare fluid particle velocity profiles across a fluid-filled channel of width $10\bar{\delta}_s$ for rigid and steel walls, neglecting thermal effects. Figure 11, for air, shows no discernable difference in the behavior of the two wall types. The same is also true of the x-component of fluid particle velocity when the channel is filled with water. This is evident from the upper plot of Fig. 12. However, the lower plot of Fig. 12 shows that, for a water-filled channel, replacing the rigid wall with steel leads to a substantial change in the behavior of the y-component of fluid particle velocity. Indeed, for a steel-walled channel, $|u_y|$ is so much greater than that found for a rigid-walled channel that the plot of $|u_y|$ for the latter is only just observable at the bottom of the figure. Note that $|u_y| \not\to 0$ on the steel-walls. We observe that whilst in an air-filled channel, the steel wall may be regarded as rigid, this is not so when the channel is filled with water.

Similar behavior is seen for a much narrower channel as illustrated in Fig. 13 for a water-filled channel of width $\bar{\delta}_s/2$. Although not shown, for an air-filled channel, there is again no discernable difference between steel and rigid-walled channels.

Figure 14 shows the evolution of elastic-velocity with distance $\bar{y}_s$ from the channel wall for the case of a water-filled channel of width $\bar{\delta}_s/2$, noting that the elastic-velocity at the channel wall ($\bar{y}_s = 0$) matches that within the fluid of

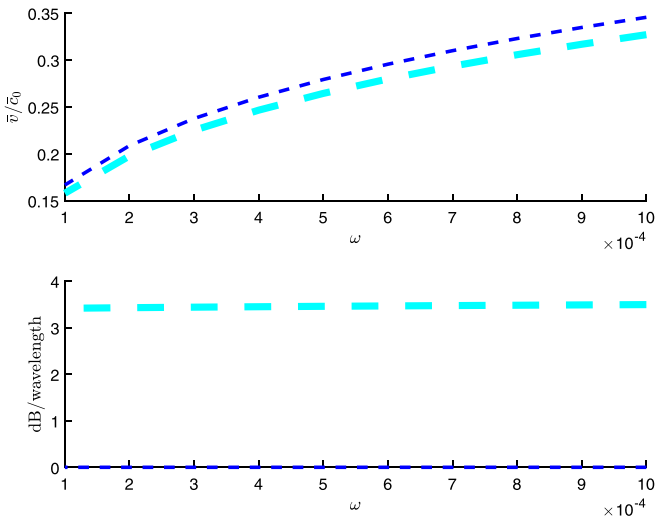

FIG. 10. (Color online) Phase speed and attenuation along a water filled channel of fixed width $\bar{\delta}_s/\bar{W} = 1$ as a function of the non-dimensional frequency ω. The long-dashed cyan curves are associated with a water-filled channel including viscosity. The short-dashed blue curves are associated with a water-filled channel neglecting viscosity. The exterior elastic medium is steel. Thermal effects are neglected.

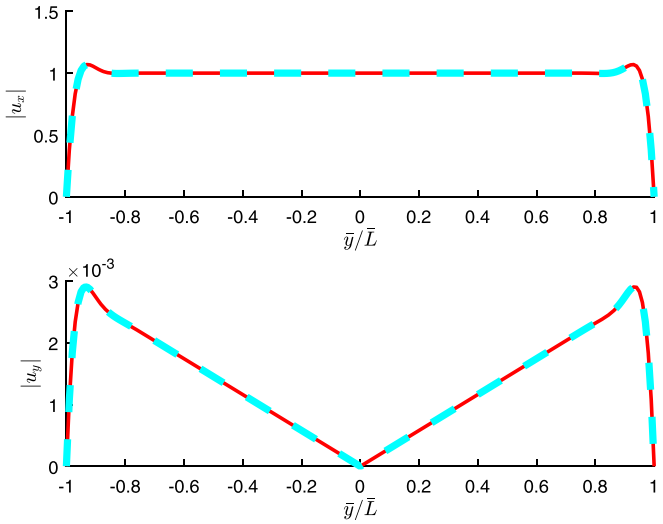

FIG. 11. (Color online) Magnitude of fluid particle velocity across an air-filled channel at 10 kHz for a channel width of $10\bar{\delta}_s$. The upper plot shows the x-component of fluid-particle-velocity, and the lower plot shows the y-component. $\boldsymbol{u}$ is normalized, independently for each boundary condition, such that $u_x(y=0)=1$. The solid-red curves indicate results associated with a rigid-walled channel, and the dashed-cyan curves are for a steel-walled channel. Thermal effects are neglected.

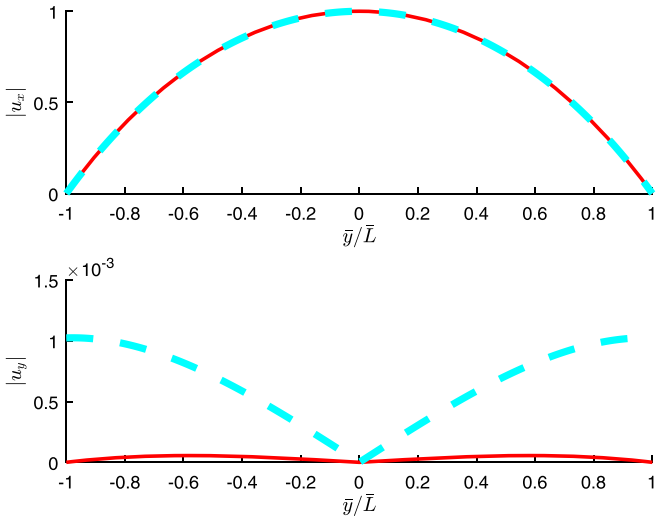

FIG. 13. (Color online) Magnitude of fluid particle velocity across a water-filled channel at 10 kHz for a channel width of $\bar{\delta}_s/2$. The upper plot shows the x-component of fluid-particle-velocity, and the lower plot shows the y-component. $\boldsymbol{u}$ is normalized, independently for each boundary condition, such that $u_x(y=0)=1$. The solid-red curves indicate a rigid-walled channel, and the dashed-cyan curves are for a steel-walled channel. Thermal effects are neglected.

Fig. 13 at $\bar{y}/\bar{L}=1$. It is clear that the elastic-velocity decays rapidly with increasing distance from the wall and hence the elastic waves associated with this mode do not carry energy away from the channel as surmised in Sec. V C 1.

It is perhaps worth considering in a little detail the nature of the propagating wave in a water-filled elastic-walled channel. For a semi-infinite elastic body, it is well known since the work of Lord Rayleigh that waves confined to its free surface can propagate without attenuation at a speed slightly less than that of shear body waves. If an inviscid fluid occupies the space above the elastic body, then the Rayleigh wave becomes *leaky* because its speed is greater than the wave speed in the fluid (i.e., it is supersonic). That is, energy is shed into acoustic waves above the solid, and hence the wave becomes attenuating. However, there is another wave at fluid/solid boundaries, called the Scholte wave, which is subsonic in both media and propagates without loss along the interface, decaying exponentially away from the boundary into both fluid and solid domains. It is found (Zhu *et al.*, 2004) that Scholte waves are not easily excited, as most of the energy is confined to the fluid region; the higher the acoustic impedance of the fluid, the stronger the Scholte wave becomes for a given forcing. Hence, for an air-steel interface, one expects to see near the surface that the Rayleigh waves dominate; they will leak energy slowly

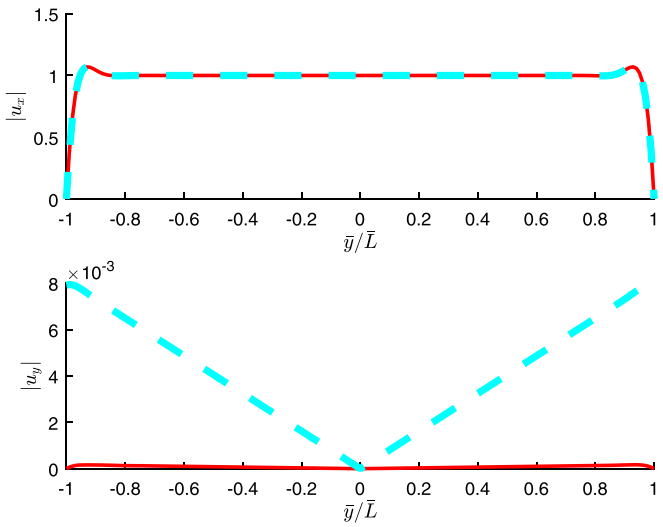

FIG. 12. (Color online) Magnitude of fluid particle velocity across a water-filled channel at 10 kHz for a channel width of $10\bar{\delta}_s$. The upper plot shows the x-component of fluid-particle-velocity, and the lower plot shows the y-component. $\boldsymbol{u}$ is normalized, independently for each boundary condition, such that $u_x(y=0)=1$. The solid-red curves indicate results associated with a rigid-walled channel, and the dashed-cyan curves are for a steel-walled channel. Thermal effects are neglected.

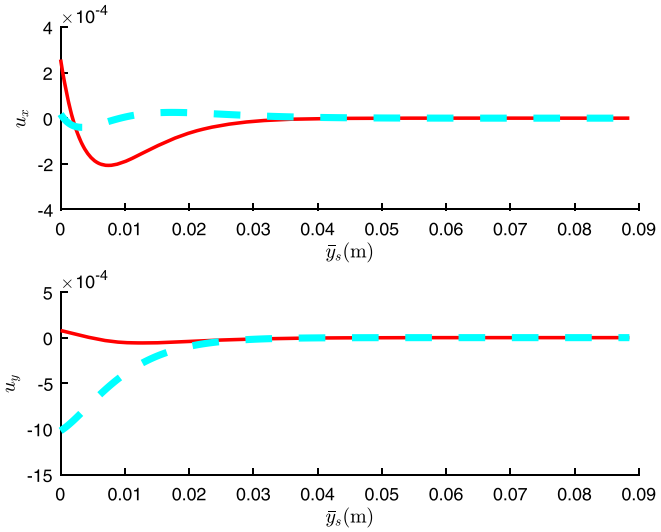

FIG. 14. (Color online) Steel wall velocity external to a water-filled channel at 10 kHz and $\bar{W}=\bar{\delta}_s/2$. The upper plot shows the x-component of particle-velocity, and the lower plot shows the y-component. In these plots, $\bar{y}_s$ denotes the dimensional distance from the channel wall within the solid. The velocity $\boldsymbol{u}$ is normalized such that $u_x=1$ at the center of the fluid-filled channel. The solid-red curves indicate the real part of velocity, and the dashed-cyan curves show the imaginary part. Thermal effects are neglected.

and the Scholte waves will be negligible. For water and steel, the Rayleigh waves will attenuate strongly due to radiation loss and Scholte waves will be more strongly excited.

The situation can be expected to be somewhat similar for water- or air-filled channels in steel; however, the leaky Rayleigh waves in both cases cannot radiate acoustic energy due to confinement and so will persist. However, the channel must be wide enough to allow the shed acoustic waves to propagate, or conversely, if the channel is too narrow, the coupled duct-Rayleigh wave mode will be cut-off. A numerical examination of the dispersion equation for the water-filled steel-walled channel indicates that at 10 kHz, the coupled duct-Rayleigh wave mode is cut-off for channel widths less than about $35\bar{\delta}_s$; we can then expect to find only a Scholte-type propagating wave mode in the water-filled steel-walled channel. This is consistent with results presented in Figs. 13 and 14 where most of the motion (and hence energy) is confined to the fluid region. Note that the presence of viscosity in the fluid means that the mode is attenuating along the channel, but otherwise it has little effect on the phase speed of the mode, as already seen.

VI. CONCLUSIONS

A general framework has been presented with which one can study the influence of thermal and viscous effects on acoustic propagation in narrow channels or ducts filled with an arbitrary Newtonian fluid. Of specific interest here was to put the experimental results of Ward *et al.* (2015) on a formal theoretical footing and better understand their conclusions regarding the influence of the boundary layer on the attenuation of acoustic waves in channels. Furthermore, of great importance as regards applications was to extend this analysis to the consideration of thermo-visco acoustic propagation in water. The theoretical analysis presented indicates that it is *Stokes's* boundary layer thickness that gives a proper indication of the extent to which acoustic propagation along narrow channels is influenced by thermal and viscous boundary effects. The parameter $\bar{\delta}_\nu$ considered in the work of Ward *et al.* (2015) is an underestimate of the extent of the influence of the boundary layer and this therefore explains the effect that was noted in the analysis of the experimental results presented there. In the context of propagation *in-air*, it has been demonstrated here that thermal effects can be significant in a channel with thermally conducting walls, but they are negligible if the wall is thermally insulating. As should be expected, the results presented in Ward *et al.* (2015) sit between these two idealized cases. Turning to the context of acoustic propagation in the channel when it is water filled, it has been shown here that any associated thermal effects are always negligible thanks to the extremely low coefficient of thermal expansion of water.

For *rigid-walled* channels, filled with low viscosity fluids such as air and water, we find that the behavior of the lowest order symmetric duct-mode is captured by simple analytic expressions, one for each of the two channel-wall thermal boundary conditions that were considered. These expressions, valid up to at least 1 MHz in air and 50 MHz in water, demonstrate explicitly that for the thermally insulating boundary condition, the complex phase speed along the channel, $v = \bar{v}/\bar{c}_0$, is independent of thermal effects. Indeed, it depends only upon the channel's width relative to the viscous boundary layer parameter, $\bar{\delta}_\nu$; that is, v depends only upon the dimensionless parameter $\bar{L}/\bar{\delta}_\nu$, with the latter containing all of the frequency dependence of v. For the thermally conducting boundary condition, we find that in addition to $\bar{L}/\bar{\delta}_\nu$, v depends upon the Prandtl number, Pr, and the dimensionless parameter, $\mathcal{A} - 1 = \beta^2/c_p = (\bar{\beta}^2\bar{T}_0\bar{c}_0^2)/\bar{c}_p$; if $\sqrt{1/\mathrm{Pr}}\,(\beta^2/c_p)$ is small, as is the case for water, thermal effects are negligible.

An important aspect that *must* be taken into account for water-filled channels is the effect of the fluid-structure interaction associated with the channel wall. Although for the *in-air* context all boundaries can be considered as perfectly rigid, it is well known that the *in-water* situation cannot be treated with such a simplification. Attenuation of acoustic energy from the channel is thereby achieved via both viscous and radiative mechanisms (i.e., energy flux into the surrounding elastic medium). Only modal solutions in the channel have been considered here, therefore the partition of this attenuated energy into viscous and radiated parts was not discussed; there is a need to investigate this when considering *forced* problems, and this shall be the focus of future work. The latter shall also examine the cut-on of possible coupled duct-Rayleigh wave modes, and the partition of energy between this and the present Scholte-type channel mode.

For the present study of the lowest order symmetric duct mode, we find that for a water-filled channel in steel, the interaction between water and the steel-wall dramatically reduces the phase speed of the mode, even when the water is treated as inviscid. For example, in a channel whose width is on the order of $\bar{\delta}_s$, the phase speed reduces by approximately 70% at a frequency of 10 kHz. The introduction of viscosity has little further impact upon phase speed, but when the reduction in phase-speed arising from fluid-structure interaction is combined with viscous losses due to boundary layer effects, we find that the mode's attenuation, in dB m^{-1}, is much greater than it would be for a rigid-walled channel. For example, at 10 kHz and a channel width of order $\bar{\delta}_s$, the attenuation increases from about 37 dB m^{-1} in a rigid-walled channel to over 77 dB m^{-1} in a steel-walled channel.

We close by commenting that although the main focus of this study has been to investigate the differences between thermo-viscous acoustic propagation in air and water-filled channels, the general theoretical framework presented here for arbitrary Newtonian fluids and elastic walls permits future study of more general configurations. Further studies on higher order modes can also be conducted although the study here of the leading order symmetric mode already indicates key, important differences between the air-filled and water-filled scenarios.

ACKNOWLEDGMENTS

This work was carried out under the Thales UK SMART Hub 2 agreement. W.J.P. acknowledges the EPSRC for funding his research fellowship (EP/L018039/1). I.D.A. undertook part of this work whilst in receipt of a Royal Society Wolfson Research Merit Award, and part was supported by the Isaac Newton Institute under EPSRC Grant No. EP/R014604/1. E.G.-N. acknowledges the EPSRC and Thales UK for funding via a KTN Industrial CASE PhD Studentship. The authors are grateful to Ward *et al.* for permission to reproduce their data (Ward *et al.*, 2015).

APPENDIX: NOTATION

Table II summarizes the notation employed.

TABLE II. Table summarizing notation employed, noting that quantities with an over-bar are dimensional and those without are non-dimensional.

$\bar{L}$	Channel half-width
$\bar{\mathcal{L}}$	Problem specific length scale (set to $\bar{L}$ for the channel problem)
$\bar{T}_0, \bar{T}$, $\theta = (\bar{T} - \bar{T}_0)/\bar{T}_0$	Ambient, total and fractional fluctuation of the fluids temperature
$\bar{\rho}_0$, $\bar{\rho}, s = (\bar{\rho} - \bar{\rho}_0)/\bar{\rho}_0$	Ambient, total and fractional fluctuation (condensation) of the fluid's density
$\bar{p}_0, \bar{p}$, $p = (\bar{p} - \bar{p}_0)/(\bar{\rho}_0 \bar{c}_0^2)$	Ambient, total and non-dimensional acoustic pressure of the fluid
$\bar{c}_0$	Adiabatic sound speed of the fluid
$\bar{\omega}, \omega = \bar{\omega}\bar{\mathcal{L}}/\bar{c}_0$	Radian frequency and non-dimensional counterpart
$\bar{c}_p, c_p = \bar{T}_0 \bar{c}_p/\bar{c}_0^2$	Specific heat at constant pressure of the fluid and non-dimensional counterpart
$\bar{\beta}$, $\beta = \bar{\beta}\bar{T}_0$	Coefficient of thermal expansion of the fluid and non-dimensional counterpart
$\mathcal{A} = 1 + \beta^2/c_p$,	Non-dimensional parameter associated with β and c_p
$\bar{\eta} = \bar{\rho}_0 \bar{c}_0 \bar{\mathcal{L}} \eta$, $\bar{\eta}' = \bar{\rho}_0 \bar{c}_0 \bar{\mathcal{L}} \eta'$	First (shear) and second coefficients of fluid viscosity
$\bar{\eta}_B = \bar{\eta}' + 2/3\bar{\eta}$ $= \bar{\rho}_0 \bar{c}_0 \bar{\mathcal{L}} \eta_B$	Bulk fluid viscosity
$\zeta = 2\eta + \eta'$ $= \eta_B + (4/3)\eta$	Non-dimensional viscosity parameter
$\bar{\nu} = \bar{\eta}/\bar{\rho}_0$	Kinematic viscosity of the fluid
$\bar{\delta}_\nu = \sqrt{\bar{\nu}/\bar{\omega}}$,	Viscous boundary layer parameter
$\bar{\delta}_s = 2\pi\sqrt{2}\,\bar{\delta}_\nu$	Stokes' boundary layer parameter
$\bar{h}_0, \bar{h}$, $h = \bar{T}_0(\bar{h} - \bar{h}_0)/\bar{c}_0^2$	Ambient, total and non-dimensional fluctuation of the fluid's entropy
$\bar{\mathcal{K}}, \mathcal{K} = \bar{T}_0 \bar{\mathcal{K}}/(\bar{\rho}_0 \bar{c}_0^3 \bar{\mathcal{L}})$	Coefficient of thermal conductivity of the fluid and non-dimensional counterpart
$\mathcal{C} = \mathcal{K}/c_p$	Non-dimensional thermal diffusion coefficient of the fluid
$\lambda = \bar{\lambda}/(\bar{\rho}_0 \bar{c}_0^2)$, $\mu = \bar{\mu}/(\bar{\rho}_0 \bar{c}_0^2)$	Lamé's elastic and shear modulus
$\rho_s = \bar{\rho}_s/\bar{\rho}_0$	Solid density
$\bar{v}_p, v_p = \bar{v}_p/\bar{c}_0$	Compressional wave-speed of the solid and non-dimensional counterpart
$\bar{v}_s, v_s = \bar{v}_s/\bar{c}_0$	Shear wave-speed of the solid and non-dimensional counterpart
κ_1, κ_2	Coupled thermo-compressional wavenumbers of the fluid
$\gamma_j = (k^2 - \kappa_j^2)^{1/2}$, $j = 1,2$	Arises in argument of thermo-compression solution, given e^{ikx} dependence
$\alpha = (k^2 - i\omega/\eta)^{1/2}$	Arises in argument of vorticity solution, given e^{ikx} dependence
$\kappa_p = \omega/v_p$, $\kappa_s = \omega/v_s$	Non-dimensional compressional and shear elastic wavenumbers
$\gamma_p = (k^2 - \kappa_p^2)^{1/2}$	Arises in argument of compressional elastic solution, given e^{ikx} dependence
$\gamma_s = (k^2 - \kappa_s^2)^{1/2}$	Arises in argument of shear elastic solution, given e^{ikx} dependence
Ω	z component of vorticity $\boldsymbol{\Omega} = \nabla \times \mathbf{u} = \Omega\hat{\mathbf{k}}$
$\phi = \nabla \cdot \boldsymbol{w}$	Compressional elastic potential (dilation)
ψ	z component of shear elastic potential, $\boldsymbol{\psi} = \nabla \times \boldsymbol{w} = \psi\hat{\mathbf{k}}$
$\bar{\boldsymbol{\sigma}} = \bar{\rho}_0 \bar{c}_0^2 \boldsymbol{\sigma}$	Viscous stress tensor
$\bar{\boldsymbol{u}} = \bar{c}_0 \boldsymbol{u}$	Fluid particle velocity
$v = \bar{v}/\bar{c}_0 = \omega/k$	Phase speed along channel
$\bar{\boldsymbol{w}} = \bar{L}\boldsymbol{w}$	Elastic displacement
$\bar{W} = 2\bar{L}$	Channel width

Allard, J., and Atalla, N. (**2009**). *Propagation of Sound in Porous Media: Modelling Sound Absorbing Materials* (Wiley, New York).

Baik, K., Jiang, J., and Leighton, T. G. (**2010**). "Acoustic attenuation, phase and group velocities in liquid-filled pipes: Theory, experiment, and examples of water and mercury," J. Acoust. Soc. Am. **128**(5), 2610–2624.

Batchelor, G. K. (**2000**). *An Introduction to Fluid Dynamics* (Cambridge University Press, Cambridge, UK).

Beltman, W. (**1999a**). "Viscothermal wave propagation including acousto-elastic interaction, Part I: Theory," J. Sound Vib. **227**(3), 555–586.

Beltman, W. (**1999b**). "Viscothermal wave propagation including acousto-elastic interaction, Part II: Applications," J. Sound Vib. **227**(3), 587–609.

Bruneau, M., Herzog, P., Kergomard, J., and Polack, J. (**1989**). "General formulation of the dispersion equation in bounded visco-thermal fluid, and application to some simple geometries," Wave Motion **11**(5), 441–451.

Christensen, J., Martin-Moreno, L., and Garcia-Vidal, F. J. (**2008**). "Theory of resonant acoustic transmission through subwavelength apertures," Phys. Rev. Lett. **101**(1), 014301.

Del Grosso, V. (**1971**). "Analysis of multimode acoustic propagation in liquid cylinders with realistic boundary conditions–application to sound speed and absorption measurements," Acta Acust. united Acust. **24**(6), 299–311.

Dokumaci, E. (**2014**). "On the effect of viscosity and thermal conductivity on sound propagation in ducts: A re-visit to the classical theory with extensions for higher order modes and presence of mean flow," J. Sound Vib. **333**(21), 5583–5599.

Dunn, F., Hartmann, W., Campbell, D., and Fletcher, N. (**2015**). *Springer Handbook of Acoustics* (Springer, New York).

Elvira-Segura, L. (**2000**). "Acoustic wave dispersion in a cylindrical elastic tube filled with a viscous liquid," Ultrasonics **37**(8), 537–547.

Estrada, H., Candelas, P., Uris, A., Belmar, F., De Abajo, F. G., and Meseguer, F. (**2008**). "Extraordinary sound screening in perforated plates," Phys. Rev. Lett. **101**(8), 084302.

Feynman, R. P., Leighton, R. B., and Sands, M. (**1965**). *The Feynman Lectures on Physics, Vol. II, Quantum Mechanics 1-1* (California Institute of Technology, Pasadena, CA).

Gomperts, M. C., and Kihlman, T. (**1967**). "The sound transmission loss of circular and slit-shaped apertures in walls," Acta Acust. united Acust. **18**(3), 144–150.

Gompeters, M. C. (**1964**). "The 'sound insulation' of circular and slit-shaped apertures," Acta Acust. united Acust. **14**(1), 1–16.

Helmholtz, H. (**1863**). "On the influence of friction in the air on sound motion," Verhandl. Naturhist. Med. Ver. Heidelberg **3**, 16–20.

Jiménez, N., Cox, T. J., Romero-García, V., and Groby, J.-P. (**2017**). "Metadiffusers: Deep-subwavelength sound diffusers," Sci. Rep. **7**(1), 5389.

Jiménez, N., Huang, W., Romero-García, V., Pagneux, V., and Groby, J.-P. (**2016**). "Ultra-thin metamaterial for perfect and quasi-omnidirectional sound absorption," Appl. Phys. Lett. **109**(12), 121902.

Kirchhoff, G. (**1868**). "Ueber den einfluss der wärmeleitung in einem gase auf die schallbewegung" ("On the effect of heat conduction on the propagation of sound waves"), Ann. Phys. **210**(6), 177–193.

Kundt, A. (**1868**). "Untersuchungen über die schallgeschwindigkeit der luft in röhren" ("Studies on the sound speed of air in pipes"), Ann. Phys. **211**(11), 337–372.

Leppington, F. G., and Levine, H. (**1973**). "Reflexion and transmission at a plane screen with periodically arranged circular or elliptical apertures," J. Fluid Mech. **61**(1), 109–127.

Liangh, P., and Scarton, H. (**2002**). "Coincidence of thermoelastic and thermoviscous acoustic waves in fluid-filled elastic tubes," J. Sound Vib. **250**(3), 541–565.

Oldham, D., and Zhao, X. (**1993**). "Measurement of the sound transmission loss of circular and slit-shaped apertures in rigid walls of finite thickness by intensimetry," J. Sound Vib. **161**(1), 119–135.

Pierce, A. D. (**1978**). "Aeroacoustic fluid dynamic equations and their acoustic energy conservation corollary with O_2 and N_2 vibrational relaxation effects included," J. Sound Vib. **58**(2), 189–200.

Putra, A., and Thompson, D. J. (**2010**). "Sound radiation from perforated plates," J. Sound Vib. **329**(20), 4227–4250.

Rauch, D. (**1980**). "Seismic interface waves in coastal waters: A review," Technical Report No. SR-42, Saclant ASW Research Centre, La Spezia, Italy.
Rayleigh, J. W. S. B. (**1896**). *The Theory of Sound, Vol. 2* (Macmillan, London).
Stinson, M. (**1991**). "The propagation of plane sound waves in narrow and wide circular tubes, and generalization to uniform tubes of arbitrary cross-sectional shape," J. Acoust. Soc. Am. **89**(2), 550–558.
Stinson, M., and Champoux, Y. (**1992**). "Propagation of sound and the assignment of shape factors in model porous materials having simple pore geometries," J. Acoust. Soc. Am. **91**(2), 685–695.
Tijdeman, H. (**1975**). "On the propagation of sound waves in cylindrical tubes," J. Sound Vib. **39**(1), 1–33.
Ward, G., Lovelock, R., Murray, A., Hibbins, A., Sambles, J., and Smith, J. (**2015**). "Boundary-layer effects on acoustic transmission through narrow slit cavities," Phys. Rev. Lett. **115**(4), 044302.
Weston, D. (**1953**). "The theory of the propagation of plane sound waves in tubes," Proc. Phys. Soc. B **66**(8), 695–709.
Wilson, G. P., and Soroka, W. W. (**1965**). "Approximation to the diffraction of sound by a circular aperture in a rigid wall of finite thickness," J. Acoust. Soc. Am. **37**(2), 286–297.
Zhu, J., Popovics, J. S., and Schubert, F. (**2004**). "Leaky Rayleigh and Scholte waves at the fluid-solid interface subjected to transient point loading," J. Acoust. Soc. Am. **116**(4), 2101–2110.
Zwikker, C., and Kosten, C. (**1949**). *Sound Absorbing Materials* (Elsevier, Amsterdam, the Netherlands).